iScience

CellPress

Article

Immunogenomic Landscape Contributes to Hyperprogressive Disease after Anti-PD-1 Immunotherapy for Cancer

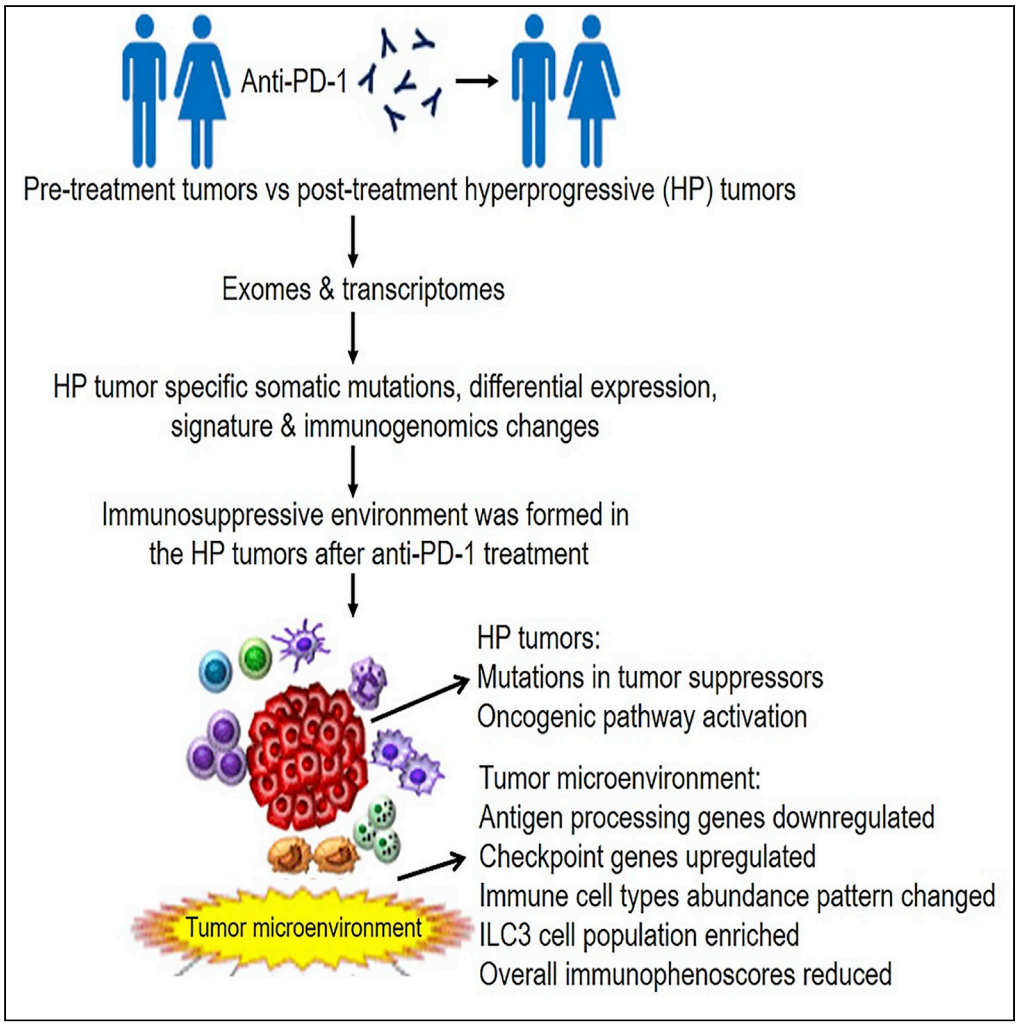

Donghai Xiong, Yian Wang, Arun K. Singavi, Alexander C. Mackinnon, Ben George, Ming You

myou@mcw.edu

HIGHLIGHTS

Mutations/expression changes occur in hyperprogressive tumors after anti-PD-1 therapy

Immune cell population abundance pattern changed in the hyperprogressive tumors

ILC3 cells may be enriched in the hyperprogressive tumors after anti-PD-1 therapy

Post-therapy hyperprogressive tumors were less immunogenic than pre-therapy tumors

Xiong et al., iScience 9, 258–277
November 30, 2018
https://doi.org/10.1016/j.isci.2018.10.021

iScience

CellPress

Article

Immunogenomic Landscape Contributes to Hyperprogressive Disease after Anti-PD-1 Immunotherapy for Cancer

Donghai Xiong,[1,2] Yian Wang,[1,2] Arun K. Singavi,[1,3] Alexander C. Mackinnon,[1,4] Ben George,[1,3] and Ming You[1,2,5,*]

SUMMARY

Although PD-1-blocking immunotherapies demonstrate significant therapeutic promise, a subset of the patients could develop hyperprogressive disease (HPD) with accelerated tumor growth after anti-PD1 immunotherapy. To elucidate the underlying mechanisms, we compared the mutational and transcriptional landscapes between the pre- and post-therapy tumors of two patients developing HPD after anti-PD-1 immunotherapy. In post-therapy HPD tumors, somatic mutations were found in known cancer genes, including tumor suppressor genes such as *TSC2* and *VHL*, along with transcriptional upregulation of oncogenic pathways, including IGF-1, ERK/MAPK, PI3K/AKT, and TGF-β. We found that post-therapy HPD tumors were less immunogenic than pre-therapy tumors, concurrent with an increased presence of ILC3 cells, a subset of innate lymphoid cells. We also developed a gene expression signature predictive of HPD. In summary, we identified the genomics and immune features associated with HPD, which may help identify patients at risk of adverse clinical outcome after anti-PD-1 immunotherapy.

INTRODUCTION

Immune checkpoint therapies including those targeting PD-1, or its primary ligand PD-L1, have demonstrated therapeutic responses across a broad range of cancer types (Sharma and Allison, 2015). Anti-PD-1 therapy blocks the interaction of PD-1, an inhibitory receptor on tumor-infiltrating T cells, with its ligands PD-L1 and PD-L2 that are predominantly expressed on tumor cells and antigen-presenting cells (APCs), respectively (Topalian et al., 2012). Despite the success of anti-PD-1 immunotherapy in approximately 20%–30% of patients with cancer, the majority of patients do not respond to this treatment (Sharma et al., 2017). In addition, increasing clinical evidence suggests that a significant subset of nonresponsive patients may experience acceleration of disease progression after treatment with anti-PD-1, a phenomenon known as hyperprogressive disease (HPD). Although accurate identification of the frequency of patients developing HPD has been limited by variability in diagnostic criteria, conservative estimates suggest that HPD may occur in as many as 10% of patients treated with anti-PD-1 (Champiat et al., 2017; Kato et al., 2017; Saada-Bouzid et al., 2017).

In contrast to identifying factors that predict responsiveness to PD-1-blocking therapies such as tumor expression of PD-L1, high tumor mutational burden, and the presence of tumor-infiltrating CD8+ T cells, little is known about the mechanisms underlying HPD. Although a pilot study suggested that some patients with *MDM2* family amplification or *EGFR* aberrations developed HPD after treatment with PD-1 or PD-L1 inhibitors (Kato et al., 2017), it is likely that alterations beyond those identified in that study are important in facilitating accelerated disease progression.

To comprehensively examine the mechanisms of HPD, we performed whole-exome sequencing (WES) and RNA sequencing (RNA-seq) analyses of formalin-fixed paraffin-embedded (FFPE) samples of tumors before and after anti-PD-1 therapy in patients with clinical evidence of HPD. We identified individual somatic mutations and mutation clusters associated with clonal evolution that may contribute to the accelerated tumor growth observed in HPD. We also identified characteristic decreases in HPD tumor immunogenicity. Finally, we identified a gene signature that may be predictive of HPD development. These changes were HPD patient specific, and were not found in the tumors of anti-PD-1-treated patients without HPD phenotypes from previous studies. Overall, our study identified the genomics and immune features associated with HPD tumors after anti-PD-1 immunotherapy.

[1]Cancer Center, Medical College of Wisconsin, Milwaukee, WI 53226, USA

[2]Department of Pharmacology & Toxicology, Medical College of Wisconsin, Milwaukee, WI 53226, USA

[3]Department of Medicine, Medical College of Wisconsin, Milwaukee, WI 53226, USA

[4]Department of Pathology, Medical College of Wisconsin, Milwaukee, WI 53226, USA

[5]Lead Contact

*Correspondence: myou@mcw.edu

https://doi.org/10.1016/j.isci.2018.10.021

Patient	Gender	Specimen	Cancer	Treatment	Other Clinical Phenotype	% Tumor
#1	Male	S1624794	Esophageal squamous cell carcinoma	Pre-anti-PD-1	Metastatic to lymph node	75
		S1707359	Esophageal squamous cell carcinoma	Post-anti-PD-1	Metastatic to lymph node	75
#2	Female	M16248	Clear cell renal cell carcinoma	Pre-anti-PD-1	Metastatic to the pleura and shoulder	50
		S1701860	Clear cell renal cell carcinoma	Post-anti-PD-1	Metastatic to the pleura and shoulder	75

Table 1. Characteristics of the Four FFPE Specimens from Two Patients, Consisting of Paired Pre- and Post-anti-PD-1 (Pembrolizumab) Treatment Samples

RESULTS

Mutation Patterns Are Altered in HPD Tumors after Anti-PD-1 Treatment

This study included two patients who received anti-PD-1 blockade immunotherapy. Relevant characteristics of the four FFPE tumor samples are summarized in Table 1. Paired tumor samples before and after anti-PD-1 treatment were obtained from a male patient with esophageal squamous cell carcinoma metastatic to lymph nodes (Patient 1) and from a female patient with clear cell renal cell cancer (ccRCC) that had metastasized to the bone (shoulder) and pleura (Patient 2). Following anti-PD-1 treatment that consisted of pembrolizumab (Merck), these two patients demonstrated HPD, as defined by the accelerated tumor growth rate and clinical deterioration using existing criteria (Kato et al., 2017). Each patient demonstrated progression at first radiologic evaluation (less than 2 months after anti-PD-1 therapy initiation). Before enrollment, written informed consent was obtained from all patients to use their tumor samples for research purposes. The study was approved by the Medical College of Wisconsin Institutional Review Board in accordance with federal regulations.

To understand the global changes that take place in HPD tumors after treatment with anti-PD-1, we performed mutational analysis on tumors obtained before and after treatment with pembrolizumab. We observed that Patient 1 had 195 somatic mutations before anti-PD-1 treatment and 338 somatic mutations after treatment; Patient 2 had 156 somatic mutations before treatment and 251 somatic mutations after treatment (Table S1). There were 154 and 124 common somatic mutations shared by the HPD and pre-therapy tumors for Patients 1 and 2, respectively (Figure S1). Our results were in line with another group's results showing increased tumor mutation load from baseline in PD (progressive disease) in patients with melanoma after anti-PD-1 therapy (nivolumab) initiation (Riaz et al., 2017). In the latter, the tumor mutation load was decreased in the responding patients (complete response/partial response) from baseline since nivolumab initiation, consistent with immunoediting (Riaz et al., 2017). We also analyzed the mutation profiles of these two patients in the context of known cancer genes based on a comprehensive list of cancer-related genes (downloaded from http://www.bushmanlab.org/links/genelists). There were 47 cancer genes mutated in at least one of the tumors from Patient 1 and 40 cancer genes mutated in at least one of the tumors from Patient 2 (Figure 1, Table S2). Four cancer genes (*APH1A*, *ARHGEF12*, *GPER1*, and *KIF14*) mutated in the pre-therapy tumor of Patient 1 were not mutated in the HPD tumors, suggesting that the tumor clones containing these four cancer genes were eliminated by anti-PD-1 treatment. However, the HPD tumor of Patient 1 had somatic mutations in 20 cancer genes, including *IGFBP2*, *KMT2C*, *MAP3K4*, *MUC16*, *MUC2*, *NCOR2*, and *NOTCH4*, which were not present in the pre-therapy tumors. Similar patterns were also observed for Patient 2. Four cancer genes (*APC2*, *OBSCN*, *PHLPP1*, and *SATB1*) that were mutated in the pre-therapy tumor of Patient 2 were not mutated in the post-treatment tumors, whereas the HPD tumor of Patient 2 had somatic mutations in 21 cancer genes, including *IGFBP2*, *MUC4*, *NCOR2*, *NFE2L2*, *TSC2*, and *VHL*, which were not present in the pre-therapy tumors. The identified mutations in these genes were not present in the tumors of non-HPD patients after anti-PD-1 treatment when compared with previous studies (Biton et al., 2018; Gong et al., 2017; Hanna et al., 2018; Hugo et al., 2016; Miao et al., 2018; Riaz et al., 2017; Rizvi et al., 2015; Teo et al., 2018; Yoshikawa et al., 2017; Zaretsky et al., 2016). These data indicate that the mutational landscape of tumors was significantly altered after anti-PD-1 therapy in patients who demonstrated hyperprogression after anti-PD-1 treatment.

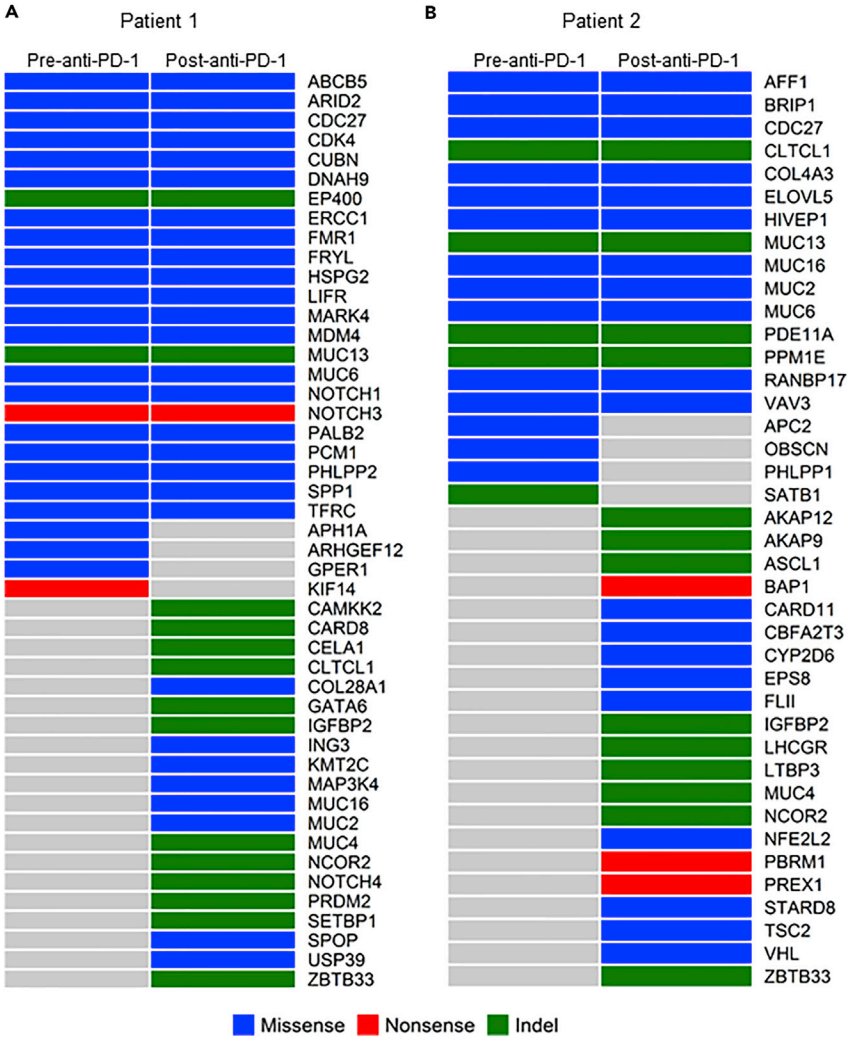

Figure 1. Profiles of Mutated Cancer Genes (Nonsilent Somatic Mutations) in the Pre- and Post-anti-PD-1 Treatment Tumor Samples

(A) Mutation pattern of Patient 1.

(B) Mutation pattern of Patient 2. Indel: insertions or deletions.

See also Figure S1, Tables S1 and S2.

For comparison in the context of corresponding cancer populations, we analyzed the numbers of somatic mutations of the esophageal carcinoma (ESCA, n = 184) and kidney renal clear cell carcinoma (KIRC, n = 384) samples from The Cancer Genome Atlas (TCGA). The numbers of nonsilent somatic mutations were in the range of 4–1,763 for ESCA and 15–1,349 for KIRC. The lower quartile, median, and upper quartile were 85, 110, and 168 for ESCA and 54, 77, and 109 for KIRC, respectively (Figure S2). The numbers of nonsilent somatic mutations in the before and after anti-PD-1 therapy tumors of the two HPD patients in this study were 195 and 338 for the patient with ESCA and 156 and 251 for the patient with KIRC. Therefore, they were all above the upper quartiles of TCGA ESCA and KIRC datasets, which suggested that these two patients have an exceptionally high number of somatic mutations compared with the TCGA esophageal cancer (ESCA) and ccRCC (KIRC).

HPD Tumors Contain Deleterious Mutations and Significantly Activated Oncogenic Signaling Pathways

To determine if certain genes were altered in both patients with HPD tumors, we searched for gene mutations that were common for the HPD tumors of both patients. Four genes were mutated in the

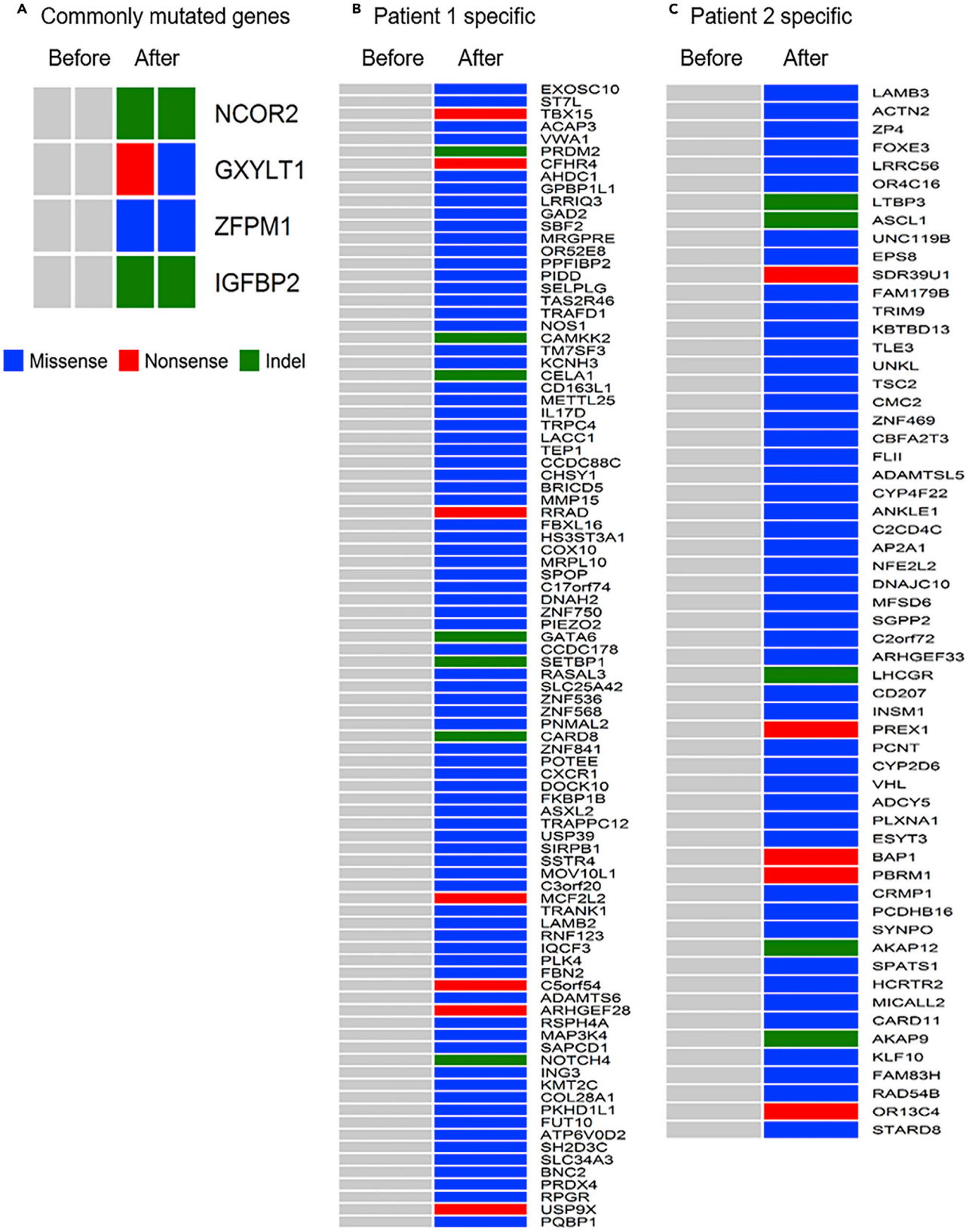
A
Commonly mutated genes
Before
After
NCOR2
GXYLT1
ZFPM1
IGFBP2
Missense
Nonsense
Indel
B
Patient 1 specific
Before
After
EXOSC10
ST7L
TBX15
ACAP3
VWA1
PRDM2
CFHR4
AHDC1
GPBP1L1
LRRIQ3
GAD2
SBF2
MRGPRE
OR52E8
PPFIBP2
PIDD
SELPLG
TAS2R46
TRAFD1
NOS1
CAMKK2
TM7SF3
KCNH3
CELA1
CD163L1
METTL25
IL17D
TRPC4
LACC1
TEP1
CCDC88C
CHSY1
BRICD5
MMP15
RRAD
FBXL16
HS3ST3A1
COX10
MRPL10
SPOP
C17orf74
DNAH2
ZNF750
PIEZO2
GATA6
CCDC178
SETBP1
RASAL3
SLC25A42
ZNF536
ZNF568
PNMAL2
CARD8
ZNF841
POTEE
CXCR1
DOCK10
FKBP1B
ASXL2
TRAPPC12
USP39
SIRPB1
SSTR4
MOV10L1
C3orf20
MCF2L2
TRANK1
LAMB2
RNF123
IQCF3
PLK4
FBN2
C5orf54
ADAMTS6
ARHGEF28
RSPH4A
MAP3K4
SAPCD1
NOTCH4
ING3
KMT2C
COL28A1
PKHD1L1
FUT10
ATP6V0D2
SH2D3C
SLC34A3
BNC2
PRDX4
RPGR
USP9X
PQBP1
C
Patient 2 specific
Before
After
LAMB3
ACTN2
ZP4
FOXE3
LRRC56
OR4C16
LTBP3
ASCL1
UNC119B
EPS8
SDR39U1
FAM179B
TRIM9
KBTBD13
TLE3
UNKL
TSC2
CMC2
ZNF469
CBFA2T3
FLII
ADAMTSL5
CYP4F22
ANKLE1
C2CD4C
AP2A1
NFE2L2
DNAJC10
MFSD6
SGPP2
C2orf72
ARHGEF33
LHCGR
CD207
INSM1
PREX1
PCNT
CYP2D6
VHL
ADCY5
PLXNA1
ESYT3
BAP1
PBRM1
CRMP1
PCDHB16
SYNPO
AKAP12
SPATS1
HCRTR2
MICALL2
CARD11
AKAP9
KLF10
FAM83H
RAD54B
OR13C4
STARD8

Figure 2. Mutation Signatures of Post-anti-PD-1 Treatment Hyperprogressor Tumors

(A–C) (A) Commonly mutated genes in the two hyperprogressor tumors, (B) specific mutated genes in Patient 1's hyperprogressor tumor, and (C) specific mutated genes in Patient 2's hyperprogressor tumor. See also Figure S1, Tables S1 and S3.

post-treatment tumors of both patients: *NCOR2*, *GXYLT1*, *ZFPM1*, and *IGFBP2* (Figure 2A). There were 96 and 64 subject-specific nonsilent somatic mutations from 154 genes in post-treatment tumors of Patients 1 and 2, respectively (Figures 2B and 2C). The detailed information of these mutations are given in Table S3.

Bioinformatics analyses of these 161 mutations led to the identification of 11 potentially deleterious somatic variants in the HPD tumors, which were predicted to be "deleterious" by SIFT, "probably damaging" by PolyPhen-2, and "potentially associated with cancer" by FATHMM (Table 2). The 11 genes having these deleterious mutations were *TRPC4*, *POTEE*, *FBN2*, *KMT2C*, *FUT10*, *PQBP1*, *TSC2*, *MFSD6*, *CYP2D6*, *VHL*, and *RAD54B*. Of the 11 mutations, 10 were located at evolutionarily conserved sites, as predicted by GERP++ (scores >2; Table 2). IPA (Ingenuity Pathway Analysis, Qiagen Inc., MD, USA), based on the 11 genes with the deleterious somatic mutations, identified a network involving these mutated genes that contributes to suppression of the *TP53* tumor suppressor and activation of *MYC*, *CCND1*, and *VEGF* oncogenes (Figure S3). The mutated *TSC2* gene carrying a missense mutation, p.Y1611S, was in the center of this network and is linked to inhibition of the TP53 pathway and activation of the MYC, CCND1, and VEGF pathways (Figure S3). TSC2 (also known as TUBERIN) is a tumor suppressor that negatively regulates cellular signaling networks that control cellular growth and proliferation (Dang et al., 2017). The MuPIT interactive protein mutation analysis (Niknafs et al., 2013) showed that the pY1611S mutation is located in the Rap/ran-GAP domain of the TSC2 protein, which is critical for the biological function of TSC2 (Figure S4). Previous studies showed that TSC2 knockdown transforms mouse and human renal epithelial cells into neoplastic stem cells that can serially propagate upon re-inoculation in mice (Dang et al., 2017). Together, it is reasonable to hypothesize that the deleterious p.Y1611S mutation could result in the loss of function of the TSC2 protein, which in turn will lead to uncontrolled proliferation of cancer cells in the HPD tumors that survive anti-PD-1 treatment.

Based on the differentially expressed genes, IPA identified four significantly activated oncogenic signaling pathways in the HPD tumors after anti-PD-1 therapy compared with the pre-therapy tumors (p value <0.01, *Z* score >2, Figure 3A). They were the insulin growth factor (IGF)-1, extracellular signal-regulated kinase (ERK)/mitogen-activated protein kinase (MAPK), Phosphatidylinositol-4,5-bisphosphate 3-kinase (PI3K)/AKT, and transforming growth factor (TGF)-β signaling pathways. A large number of genes in these oncogenic pathways were upregulated in the HPD tumors (Figure 3B). Such concerted gene expression changes may synergistically contribute to the generation of the HPD tumors after anti-PD-1 immunotherapy.

Clonal Evolution Was Detected in HPD Tumors after Anti-PD-1 Therapy

The generation of WES data allowed us to quantify the mutant allele frequencies in all cases. Based on mutation clustering results, we inferred the identity of three clones having distinct sets of mutations (clusters) in pre-therapy tumors when compared with post-therapy HPD tumors of the two patients. Multiple mutation clusters (n = 3) were present in each of the pre-therapy tumors of the two HPD patients. In Patient 1, the post-anti-PD-1 treatment HPD tumor was associated with the outgrowth of new clone(s) represented by mutations in cancer-associated genes including *KMT2C*, *NCOR2*, *COL28A1*, *ING3*, *CAMKK2*, and *CARD8* (Figures 4A and 4C). The pre-therapy tumor clone(s) characterized by mutations in *APH1A*, *ARHGEF12*, *GPER1*, and *KIF14* genes was eliminated by anti-PD-1 treatment (Figures 4A and 4C). The clone(s) represented by mutations in the cancer genes *EP400*, *CUBN*, *SPP1*, *PHLPP2*, *PALB2*, *ERCC1*, *TFRC*, *MARK4*, and *MDM4* remained stable under the selection pressure of anti-PD-1 treatment (Figures 4A and 4C). In Patient 2, the post-anti-PD-1 treatment HPD tumor was associated with the evolution of new clone(s) represented by mutations in the cancer genes including *BAP1*, *CARD11*, *CBFA2T3*, *CYP2D6*, *PBRM1*, *TSC2*, and *VHL* (Figures 4B and 4D), whereas the pre-therapy tumor clone with mutations in *APC2*, *CDC27*, *OBSCN*, *PHLPP1*, and *SATB1* was not detectable after anti-PD-1 treatment (Figures 4B and 4D). Other clones, including those represented by mutations in *COL4A3*, *TTC40*, *NPHS1*, *UGT2A3*, *RYR1*, *AGGF1*, and *LANCL1*, remained stable before and after anti-PD-1 treatment (Figures 4B and 4D).

The tumor clonal evolution pattern associated with anti-PD-1 treatment was further validated by analyzing an independent dataset from a previous study, which conducted WES of paired baseline and relapsed tumors (before and after anti-PD-1 treatment) of four patients with melanoma (Zaretsky et al., 2016). As can be

Gene	Genomic Position[a]	Genomic Mutation	Exon	Protein Alteration	Predicted Effect of Somatic Mutation				snp137	ESP MAF[f]
					SIFT[b]	PolyPhen-2[c]	FATHMM[d]	GERP++[e]		
TRPC4	chr13: 38211734	c.G2045A	10	p.R682H	Deleterious (0.00)	Probably damaging (0.999)	Potentially associated with cancer (−2.83)	6.06	NA	NA
POTEE	chr2: 132021334	c.A2306T	15	p.Y769F	Deleterious (0.00)	Probably damaging (0.997)	Potentially associated with cancer (−4.69)	NA	NA	NA
FBN2	chr5: 127666313	c.C4297T	33	p.R1433C	Deleterious (0.00)	Probably damaging (0.983)	Potentially associated with cancer (−2.9)	4.21	NA	7.70×10^{-5}
KMT2C	chr7: 151932981	c.G2690C	16	p.R897P	Deleterious (0.00)	Probably damaging (0.995)	Potentially associated with cancer (−2.21)	5.1	NA	NA
FUT10	chr8: 33246817	c.G876T	4	p.K292N	Deleterious (0.00)	Probably damaging (1.00)	Potentially associated with cancer (−4.75)	3.42	NA	NA
PQBP1	chrX: 48759773	c.C256T	4	p.P86S	Deleterious (0.00)	Probably damaging (0.996)	Potentially associated with cancer (−1.13)	5.02	NA	NA
TSC2	chr16: 2137907	c.A4832C	37	p.Y1611S	Deleterious (0.02)	Probably damaging (0.997)	Potentially associated with cancer (−3.16)	4.59	NA	NA
MFSD6	chr2: 191301728	c.G973A	3	p.G325R	Deleterious (0.00)	Probably damaging (0.998)	Potentially associated with cancer (−2.42)	6.07	NA	NA
CYP2D6	chr22: 42522990	c.C1025T	7	p.T342M	Deleterious (0.00)	Probably damaging (0.996)	Potentially associated with cancer (−2.26)	4.06	NA	NA
VHL	chr3: 10191479	c.C349G	2	p.L117V	Deleterious (0.00)	Probably damaging (0.994)	Potentially associated with cancer (−6.95)	3.07	NA	NA
RAD54B	chr8: 95411747	c.T721G	6	p.F241V	Deleterious (0.01)	Probably damaging (0.996)	Potentially associated with cancer (−3.01)	5.55	NA	NA

Table 2. Characteristics of the 11 Deleterious Somatic Mutations in the HPD Tumors after Anti-PD-1 Treatment

ESP, NHLBI Exome Sequencing Project; NA, not available. See also Figure S3.

[a]Genomic positions are given according to the UCSC Genome Browser hg19 reference assembly.

[b]SIFT scores range from 0 to 1. The amino acid substitution is predicted to be damaging if the score is ≤0.05 and tolerated if the score is >0.05.

[c]PolyPhen-2 scores 0.85–1 are interpreted as probably damaging, scores 0.2–0.85 are possibly damaging, and sores 0–0.2 are benign.

[d]Predictions with FATHMM scores less than 0.75 indicate that the mutation is potentially associated with cancer; otherwise the mutation is not associated with cancer.

[e]There is an indication of evolutionary conservation if a given site shows a GERP++ score >2.

[f]MAFs are according to the NHLBI GO Exome Sequencing Project (ESP6500SI-V2 release) Exome Variant Server v.0.0.21 (August 2013).

seen from Figures S5 and S6, all four melanoma cases demonstrated allele clusters after anti-PD-1 therapy. Variant allele frequencies (VAFs) of the Cluster 1 mutations were not significantly changed by PD-1 blockade; Cluster 2 mutations had reduced VAFs but were still prevalent in the relapsing tumor after PD-1 blockade; Cluster 3 mutations represented the newly evolved tumor clone(s) in the relapsing tumor after PD-1 blockade; Cluster 4 mutated genes represented the tumor clone(s) that diminished to

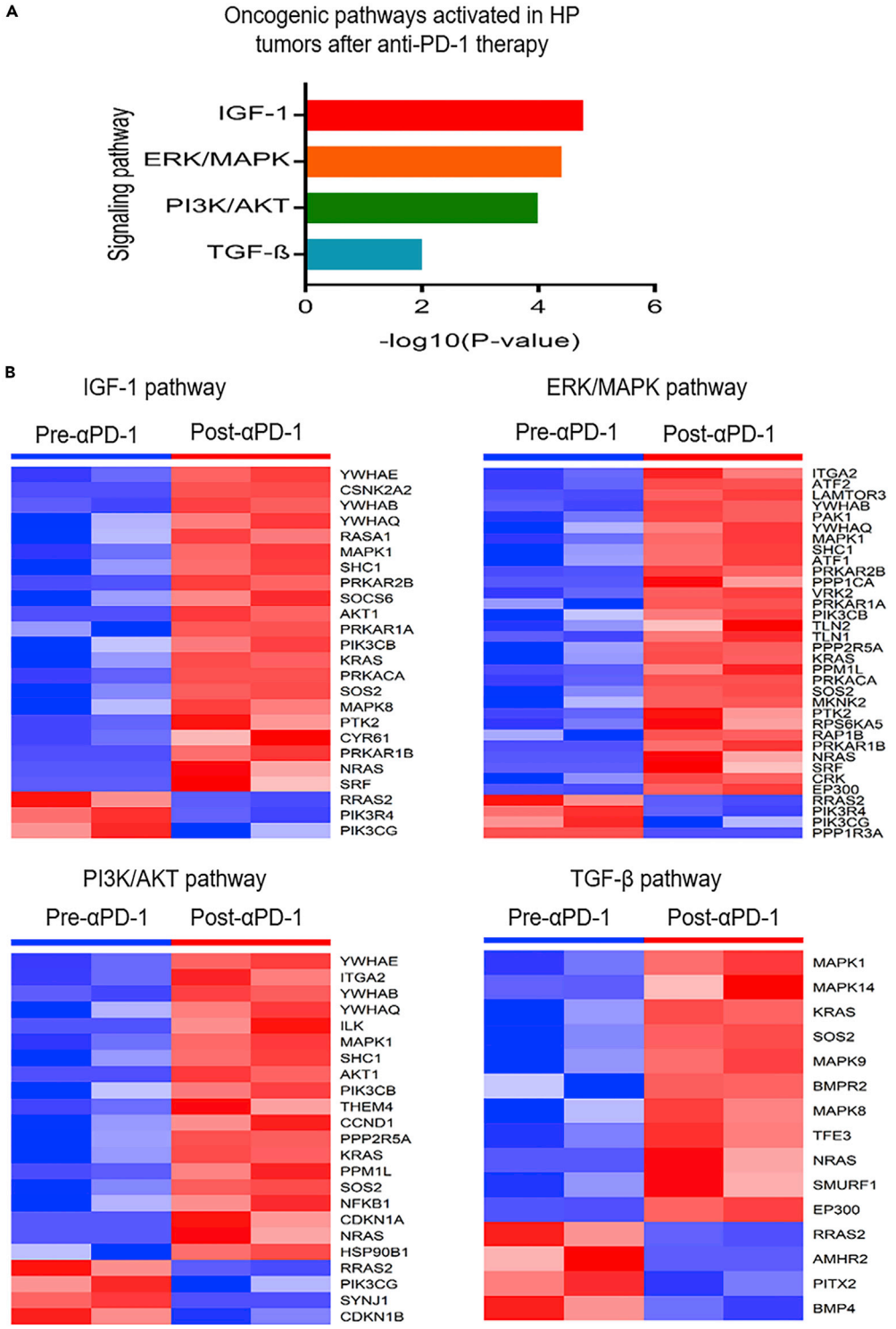

Figure 3. Activation of Oncogenic Pathways in HP Tumors after Anti-PD-1 Therapy

(A and B) (A) Four oncogenic pathways were activated in the HP tumors. (B) The differentially expressed genes in these oncogenic pathways. Most of the genes were upregulated in the HP tumors after anti-PD-1 therapy. HP, hyperprogressive.

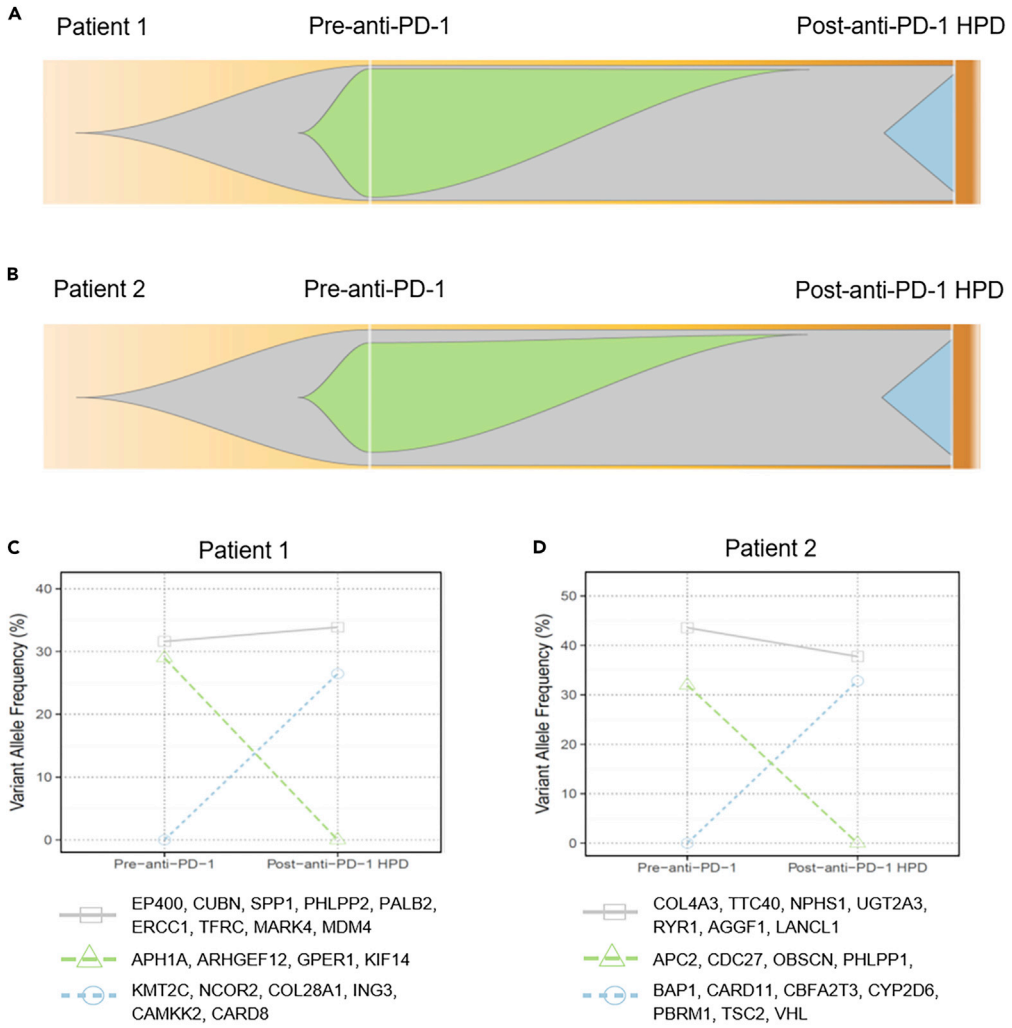

Figure 4. Illustration of Clonal Evolution of the Tumors before and after Anti-PD-1 Immunotherapy of the Two Patients with HPD

(A–D) (A) Tumor clonal evolution in Patient 1 and (B) tumor clonal evolution in Patient 2. The gray area denotes the tumor clones unaffected by anti-PD-1 therapy, the green and blue areas denote the tumor clones diminishing and appearing due to anti-PD-1 therapy. The dynamics of these clones represented by changes in the variant allele frequency between the pre- and post-therapy tumors was plotted for (C) Patient 1 and (D) Patient 2. See also Figures S5 and S6.

undetectable levels after PD-1 blockade. These data are consistent with our own analysis of tumors from HPD patients before and after anti-PD-1 therapy.

HPD Tumors Demonstrate Decreased Immunogenicity Relative to Pre-therapy Tumors

Since anti-PD-1 treatment renders its effects on tumors in a manner completely dependent on immunity, we investigated whether HPD tumors demonstrated changes in their capacity to elicit productive immune reactions using an *in silico* immunophenogram approach (Charoentong et al., 2017). The results showed that HPD tumors had much smaller immunophenoscores compared with the pre-therapy tumors for both patients (Figure 5). Expression of HLAs (human leukocyte antigens) was downregulated in the post-therapy HPD tumors compared with the pre-therapy tumors, whereas checkpoint genes were upregulated in the HPD tumors (Figure 5). These changes resulted in the overall reduction of immunophenoscores in HPD tumors. Consistent with results from the immunophenogram analysis, the differential expression analysis showed that seven genes involved in antigen processing were downregulated in the HPD tumors, i.e., *B2M*, *HLA-B*, *HLA-DPA1*, *HLA-DPB1*, *HLA-DRA*, *HLA-E*, and *HLA-F* (Figure 6A). In addition, eight genes

encoding immune checkpoints or modulators were upregulated in the HPD tumors, i.e., *CTLA4*, *KDR*, *CD96*, *CD70*, *TNFRSF18*, *TNFRSF25*, *BTNL2*, and *TNFRSF8* (Figure 6A). Changes in expression of these immune-related genes were likely contributors to the weakened immunogenicity of the HPD tumors.

Immune Cell Signatures in HPD Tumors Are Predominately Immunosuppressive

Previous studies have characterized the signature genes of 28 immune cell populations critical to immune responses across multiple cancers (Angelova et al., 2015; Charoentong et al., 2017). Using GSVA (Gene Set Variation Analysis) (Hanzelmann et al., 2013), we evaluated the immune cell landscape in the HPD tumors from our two patients. We identified that the activities of eight immune cell populations were significantly decreased in the HPD tumors after anti-PD-1 treatment (Figure 6B). These populations were monocytes, central memory CD4 T cells, immature dendritic cells, CD56dim NK (natural killer) cells, NK cells, gamma-delta (γδ) T cells, activated dendritic cells, and follicular helper T cells, most of which are linked to functional tumor clearance. In addition, the activities of three immune cell populations, i.e., neutrophils, activated B cells, and neutrophil-like myeloid-derived suppressor cells (MDSC), were upregulated in the hyperprogressors (Figure 6B). These data suggest that the depletion of monocytes, certain types of T cells, NK cells, and dendritic cells may contribute to the ability of HPD tumors to escape immune surveillance. Furthermore, the upregulated neutrophil population as well as the neutrophil-like MDSC (i.e., the MDSC subpopulation with neutrophil signature gene expression) (Zhang et al., 2017) may also contribute to the immune evasion of HPD tumors since these cell populations have been implicated in generating a milieu that attenuates immune responses in the tumor microenvironment (Galdiero et al., 2013; Mishalian et al., 2013; Sagiv et al., 2015; Tuting and de Visser, 2016; Zhang et al., 2017).

ILC3 Innate Lymphocytes Are Upregulated in HPD Tumors

Recent studies have revealed the importance of innate lymphoid cells (ILCs) in homeostasis and inflammation of tumors (Bjorklund et al., 2016; Wallrapp et al., 2017). Although three main populations of ILCs, ILC1, ILC2, and ILC3, have been categorized based on their transcription factor profiles and secreted cytokines (Spits et al., 2013), little is known about their roles in carcinogenesis and immunotherapy resistance. To evaluate ILCs in HPD tumors, we analyzed the transcriptional levels of the marker genes characteristic of the ILC1, ILC2, and ILC3 populations (Bjorklund et al., 2016; Wallrapp et al., 2017). GSEA (Subramanian et al., 2005) showed that the ILC3 marker genes were significantly enriched among the top upregulated genes in the HPD tumors after anti-PD-1 treatment (Figures 7A and 7B). In contrast, the ILC1 and ILC2 marker genes were not enriched in either the up- or downregulated genes in the HPD tumors (Figure S7). These data suggest that the ILC3 population is activated in HPD tumors. To validate this finding, we analyzed the RNA-seq data from other studies that evaluated tumor changes in response to anti-PD-1 therapies. Analysis of the transcriptomes of responding (n = 15) and nonresponding (n = 13) pre-treatment melanoma tumors from the patients subject to PD-1 blockade (Hugo et al., 2016) showed that ILC3 marker genes were commonly upregulated in the melanoma tumors resistant to anti-PD-1 therapy (Figure 7C). Based on the RNA-seq data of the $Kras^{G12D}$ mouse model, we also found that there were a large number of ILC3 marker genes significantly upregulated in murine lung adenocarcinoma tumors that were resistant to anti-PD-1 therapy when compared with untreated tumors (Koyama et al., 2016) (Figure 7D). These results are concordant with our HPD RNA-seq data, suggesting that enrichment of the ILC3 population in the HPD tumors may be a characteristic feature of tumors that are insensitive to anti-PD-1. This finding is consistent with the previous report that ILC3 lymphocytes contribute to the initiation and progression of cancers (Fung et al., 2017). The mechanistic connection between ILC3 population and anti-PD-1 therapy effect is unknown. However, it was reported that ILC3 may promote the growth of mutant tumor cells that express the receptors needed for oncogenic pathways (Fung et al., 2017; Kirchberger et al., 2013). Our and others' data (Riaz et al., 2017) suggested that anti-PD-1 therapy increased tumor mutation burden in patients with cancer with hyperprogressive or progressive tumor phenotype. Therefore, activated ILC3 cell population may be required for the promotion of the growth of more mutant cells in the patients with cancer with HPD or PD subjected to anti-PD-1 therapy.

Pro-inflammatory Pathways Were Activated in the Pre-therapy Tumors of Patients with HPD and Further Activated by Anti-PD-1 Therapy

PD-1 has been demonstrated to inhibit excessive inflammatory responses during infection in mouse models (Lazar-Molnar et al., 2010). To identify the inflammatory changes in HPD tumors, we evaluated changes in inflammatory-related genes included in the "hallmark inflammatory" gene set (Liberzon et al., 2011, 2015). To characterize the inflammation activity in post-anti-PD-1 treatment HPD tumors versus

Patient 1

Pre-therapy tumors

Immunophenoscore: 4

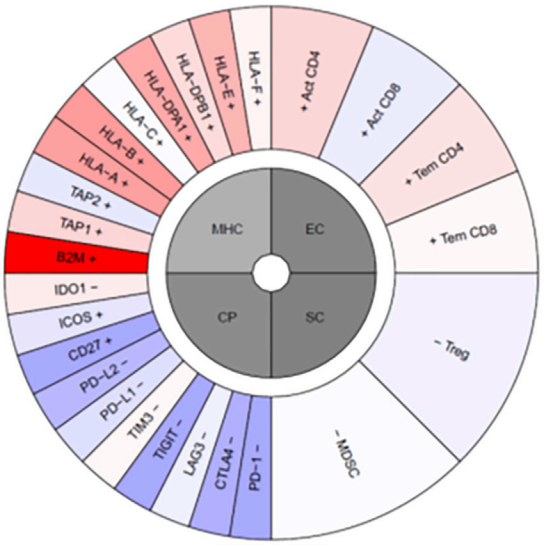

Post-αPD-1 HPD tumors

Immunophenoscore: 0

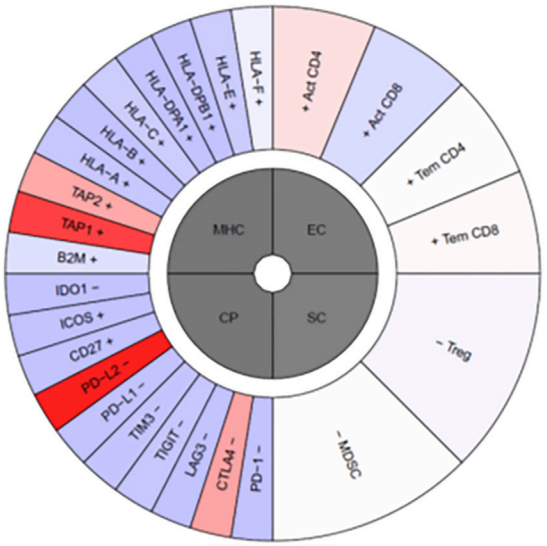

Patient 2

Immunophenoscore: 6

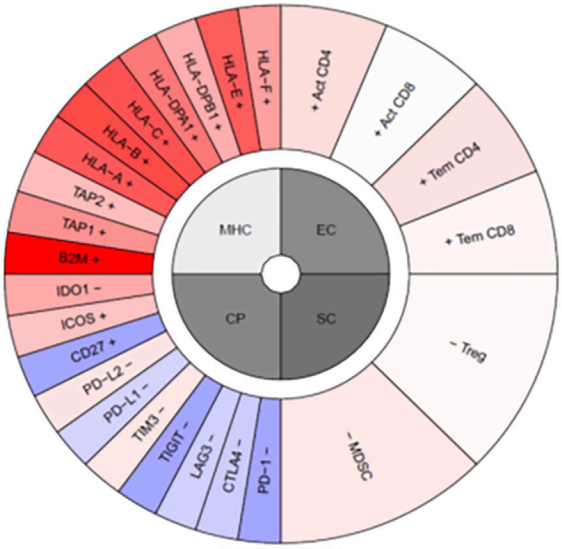

Immunophenoscore: 3

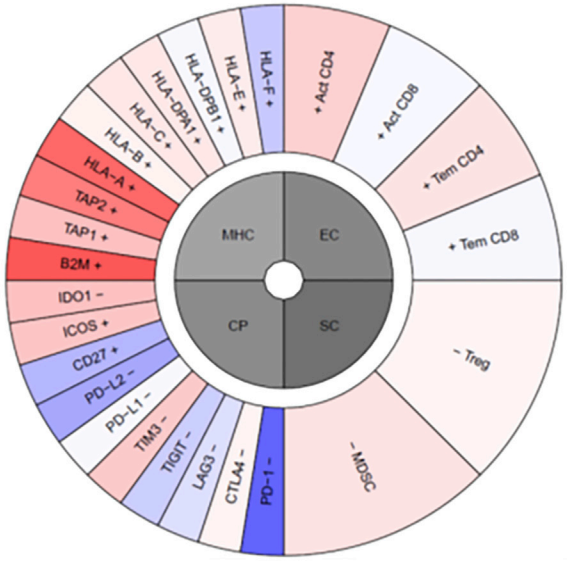

MHC: Antigen Processing

CP: Checkpoints | Immunomodulators

EC: Effector Cells

SC: Suppressor Cells

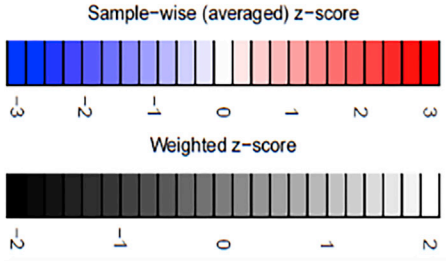

Figure 5. Immunophenoscores of the Hyperprogressor versus Non-hyperprogressor Tumors of the Two Patients Subject to Anti-PD-1 Immunotherapy

HLAs were downregulated in the HPD tumors compared with the pre-therapy tumors (shown in the upper left quadrant termed MHC), whereas checkpoints were upregulated in the HPD tumors (shown in the lower left quadrant termed CP). These changes resulted in the overall reduction of immunophenoscores in the HPD tumors resistant to anti-PD-1 immunotherapy. See also Figure S14.

pre-treatment tumors, we again utilized GSVA, which identified four founder datasets of inflammation pathways that were significantly enhanced in the HPD tumors after anti-PD-1 treatment (Figure 8A). In each of these four pro-inflammatory datasets, many more genes were up- than downregulated (Figures 8B–8E), suggesting an overall pro-inflammatory trend after anti-PD-1 treatment.

For comparison, we analyzed the gene expression data of tumor samples from the GSE52562 dataset before anti-PD-1 treatment (Westin et al., 2014). This dataset included two potential HPD patients whose progression-free survival (PFS) was less than 2 months post-pidilizumab treatment (SAMPLE.25 and SAMPLE.5 in Table S4) and four responsive patients whose PFS was more than 2 years (24 months) after treatment (SAMPLE.23, SAMPLE.19, SAMPLE.13, and SAMPLE.17 in Table S4). This analysis showed that the tumors of HPD patients have elevated inflammation pathway activity (mainly chemokine activity) even before anti-PD-1 therapy when compared with tumors from non-HPD patients (Figure S8). These and our data collectively suggested that anti-PD-1 therapy further boosts the pre-existing high levels of inflammation in patients who subsequently develop HPD in ways that are not conducive to promoting tumor rejection.

HPD-Associated Gene Expression Signature

Based on the pre-therapy tumor expression data of Dataset_1 (See Transparent Methods), we developed a 121-gene set to differentiate HPD patients from non-HPD patients (Figure S9, Table S5). The effectiveness of this 121-gene classifier in the identification of HPD patients was tested using the pre-therapy tumor expression data from Dataset_2 (See Transparent Methods). This classifier had an area under curve (AUC) value of 0.91 (95% confidence interval [CI], 0.87–0.96), a sensitivity of 71% (95% CI, 51%–87%), and a specificity of 93% (95% CI, 80%–99%) in predicting HPD patients in Dataset_2 (Figure 9A). Kaplan-Meier analysis of TCGA data showed that the 121-gene expression signature can significantly separate low-risk group from high-risk group in the 13 major types of cancers including melanoma (SKCM), glioma, and carcinomas of the esophagus (ESCA), stomach (STAD), breast (BRCA), kidney (KIRC), bladder (BLCA), liver (LIHC), head and neck (HNSC), lung (LUAD and LUSC), colon (COAD), and pancreas (PAAD) (Figures 9B–9D and S10–S12). This panel was able to identify extremely high-risk groups in ESCA, COAD, and PAAD (Figures 9B–9D).

DISCUSSION

Checkpoint blockade with anti-PD-1 antibodies has resulted in excellent responses in a subset of patients with cancer. However, there is a sizable proportion of patients with cancer who do not respond to anti-PD-1 treatment, with a subset of these patients developing hyperprogression with accelerated tumor growth after anti-PD-1 immunotherapy (Champiat et al., 2017; Kato et al., 2017). Currently, there is a lack of systematic genome studies to identify the genes or immune factors that predict resistance to immune checkpoint inhibition or HPD in response to anti-PD-1 treatment. In this study, we utilized WES and RNA-seq approaches to identify the mutation spectrum and gene expression profiling changes in HPD tumors when compared with pre-therapy tumors. We also performed pathway and tumor immunogenicity analyses based on the RNA-seq data. Finally, we combined our data with publicly available datasets and developed an HPD gene expression signature capable of predicting patients unlikely to respond to anti-PD-1.

The mutation analysis highlighted 11 genes with deleterious mutations in the HPD tumors after anti-PD-1 therapy (Table 2). Most of these genes have not been adequately studied in the context of cancer before. However, a query of this 11 mutated gene set in the cBioPortal website (http://www.cbioportal.org/) (Cerami et al., 2012; Gao et al., 2013) showed that this gene set has somatic mutations or copy number aberrations (CNAs) in 8,887 (22%) of the 41,320 sequenced patients. The alterations of these 11 genes were most frequent in the six major cancer types with an alteration frequency >30% (Figure S13), i.e., prostate cancer (70.8% tumor samples had mutations or CNAs in at least one of the 11 genes), melanoma (50.2% altered), renal cell carcinoma (45.3% altered), brain cancer (33.3% altered), breast cancer (31.1% altered), and colorectal adenocarcinoma (31.0% altered). These data support the cancer linkage to these 11 genes, the mutations of which could contribute to the tumor hyperprogressive phenotype.

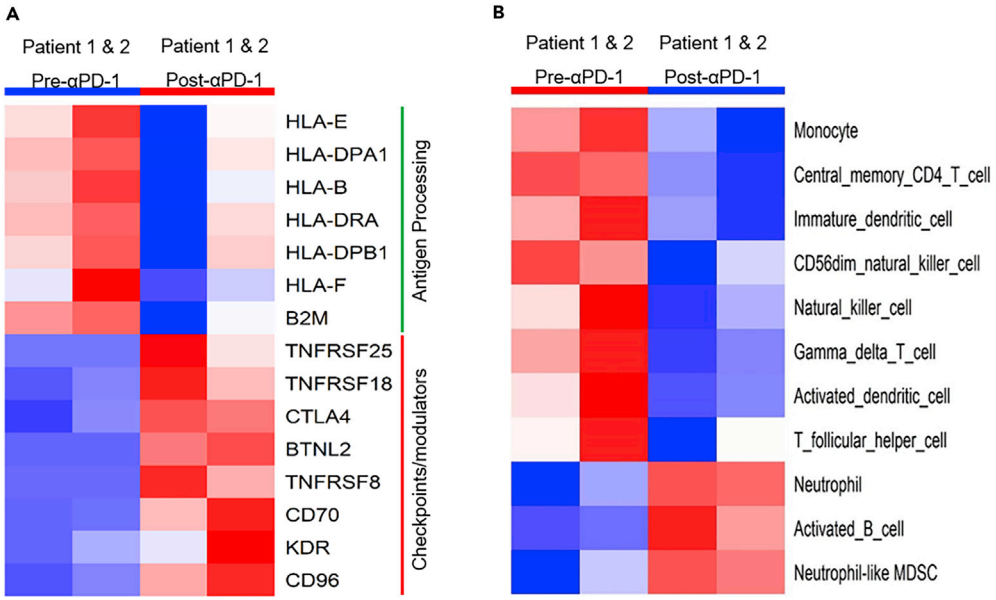

Figure 6. Changes in the Expression of Critical Immune-Related Genes and the Activity of Immune Cell Populations Contribute to Decreased Immunogenicity in the Post-α-PD-1 HPD Tumors

(A) Seven genes involved in antigen processing were downregulated, whereas eight genes encoding immune checkpoints or modulators were upregulated in hyperprogressor tumors.

(B) The activity of eight immune cell populations were weakened and three were strengthened, as detected by GSVA method.

See also Figure S14.

Among the 11 genes, some have tumor suppressive properties, good examples being *TSC2* and *VHL*. Inactivating mutations in *TSC2* that encode the protein tuberin lead to constitutive activation of mTOR kinase through the Rheb-GTP signaling axis (Menon et al., 2014; Zoncu et al., 2011), which in turn induces cell growth, motility, invasion, and development of tumors (Goncharova et al., 2004, 2006). These outcomes were consistent with our observation that the deleterious pY1611S mutation in the key Rap/ran-GAP domain of the TSC2 protein (Table 2, Figure S4) occurred in the hyperprogressive tumors after anti-PD-1 therapy. We also found that the *VHL* gene had a deleterious mutation—pL117V—in the ccRCC hyperprogressive tumors after anti-PD-1 treatment (Table 2). *VHL*, located on chromosome 3p25, is a major tumor suppressor gene involved in ccRCC oncogenesis (Gossage et al., 2015). Interestingly, a recent study found that PD-L1 expression was associated with dense PD-1 expression and wild-type *VHL* ccRCC, but not with mutated/inactivated *VHL* ccRCC (Kammerer-Jacquet et al., 2017). Therefore, only the patients with ccRCC with wild-type *VHL* may benefit from immunotherapies inhibiting PD-L1/PD-1 (Kammerer-Jacquet et al., 2017). In our case, we found that only the post-anti-PD-1 therapy hyperprogressive ccRCC tumor had detectable deleterious *VHL* mutation, but the pre-therapy ccRCC tumor did not. This suggested that the selection pressure of anti-PD-1 therapy eliminated most of the wild-type *VHL* ccRCC cells but had little effect on cells with mutated *VHL* ccRCC, such that these mutated cells were highly enriched in the post-therapy HPD tumors. This has significant implications in that it suggests that ccRCC cells with an altered/mutated *VHL* gene may be a key factor leading to HPD after anti-PD-1 therapy.

The pre- and post-treatment tumors in this study were acquired through biopsy from the primary lesion. After anti-PD-1 therapy, the initial minor subclones of somatic mutations could be boosted by the treatment and expanded in the tumor samples of the two HPD patients as shown in Figure 4, which contributed to the tumor heterogeneity that may account for changes in the mutational and/or expression landscape. Clonal evolution analysis (Figure 4) indicates that HPD tumor-specific mutations in *TSC2* and *VHL* along with mutations in a number of other cancer genes including *KMT2C*, *NCOR2*, *COL28A1*, *ING3*, *CAMKK2*, *CARD8*, *BAP1*, *CARD11*, *CBFA2T3*, *CYP2D6*, and *PBRM1* could be significant to the progression of nonaggressive pre-therapy tumors to the hyperprogressive state after anti-PD-1 treatment. Figure S3 showed that the mutated *KMT2C*, *TSC2*, *VHL*, and *CYP2D6* genes were involved in the gene-gene interaction

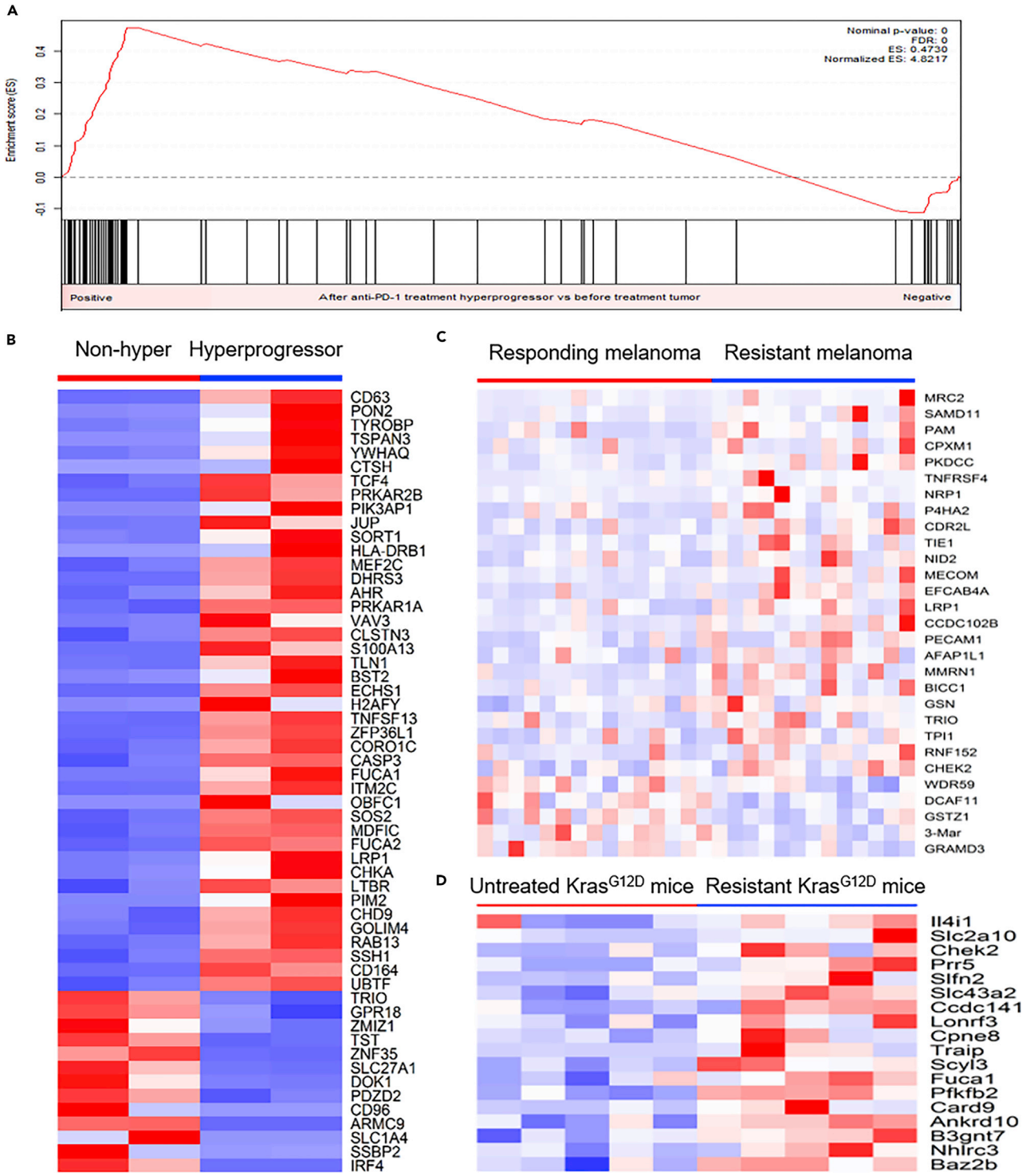

Figure 7. The ILC3 Population Was Activated in the HPD Tumors after Anti-PD-1 Therapy

(A–D) (A) GSEA showed that ILC3 marker genes were significantly enriched in the top upregulated genes in HPD tumors resistant to anti-PD-1 therapy. (B) Most of the differentially expressed ILC3 marker genes in the HPD tumors resistant to anti-PD-1 treatment were upregulated. (C) A higher percentage of ILC3 marker genes were upregulated in the nonresponding melanoma tumors resistant to anti-PD-1 therapy based on the analysis of data from an independent study in humans. (D) Upregulation of ILC3 marker genes comparing anti-PD-1-treatment-resistant mouse tumors with untreated tumors in the $Kras^{G12D}$ mouse model.

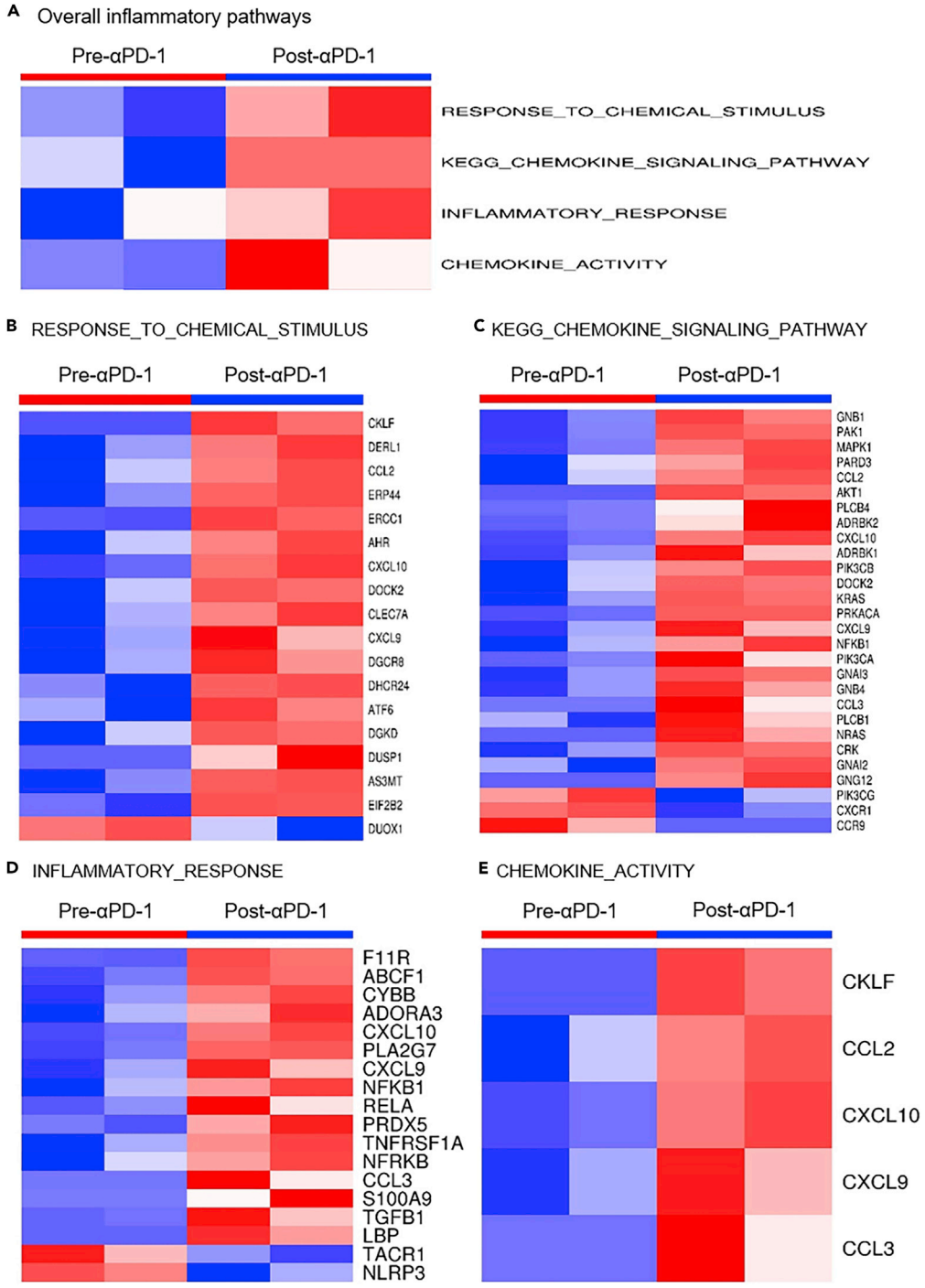

Figure 8. Activation of Inflammatory Pathways in the HPD Tumors after Anti-PD-1 Treatment

(A) GSVA identified the activation of four founder datasets of inflammation pathways.

(B) Differentially expressed genes in the inflammatory signature of RESPONSE_TO_CHEMICAL_STIMULUS;

(C) Differentially expressed genes in the inflammatory signature of KEGG_CHEMOKINE_SIGNALING_PATHWAY;

(D) Differentially expressed genes in the inflammatory signature of INFLAMMATORY_RESPONSE; (E) Differentially expressed genes in the inflammatory signature of CHEMOKINE_ACTIVITY. In each of the four pro-inflammatory datasets from (B–E), there were much more upregulated than downregulated genes. See also Figure S8.

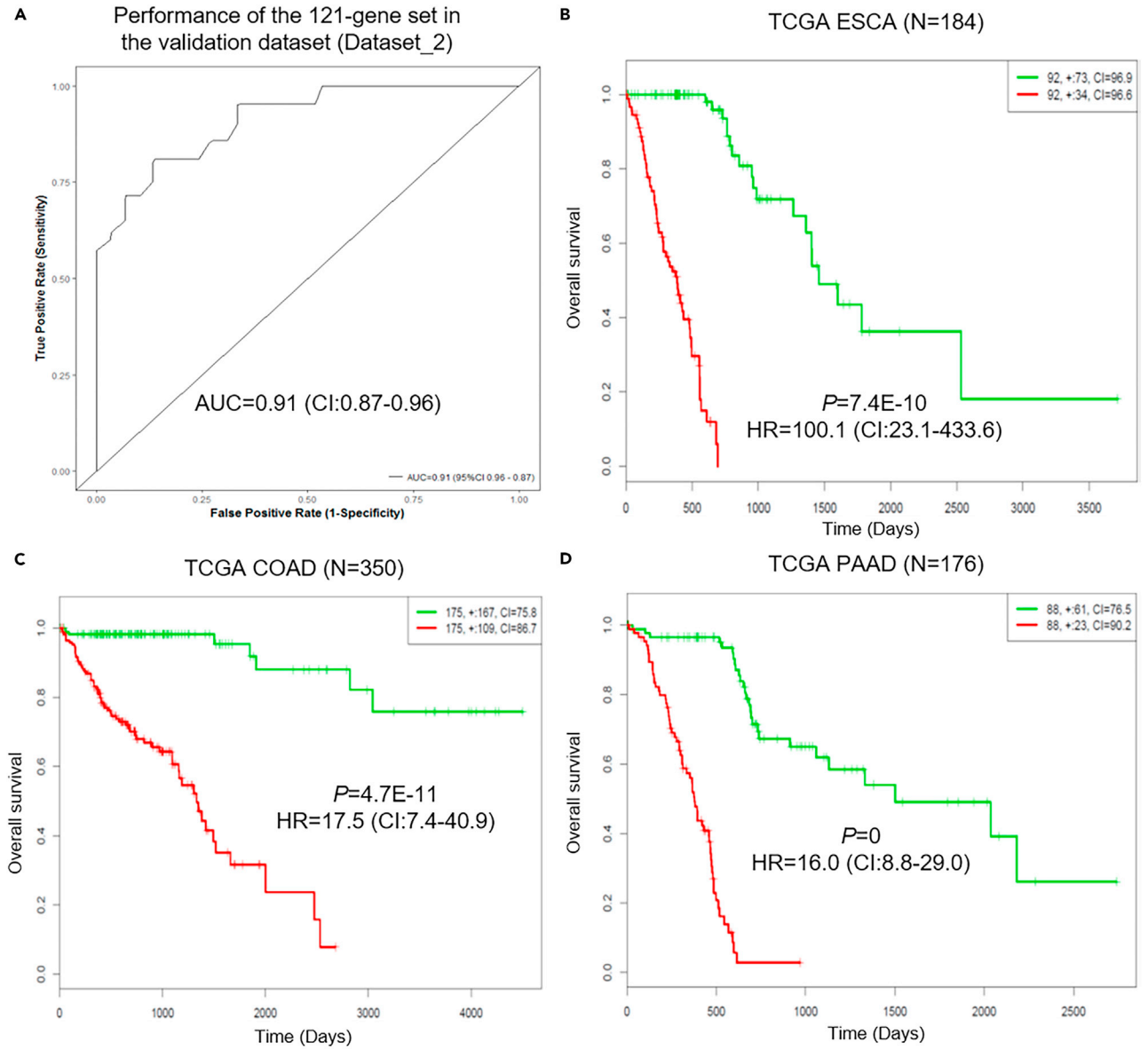

Figure 9. Performance of the 121-Gene Set Classifier in the Validation Dataset and Its Effectiveness in the Prognosis of Worse Survival Outcome in the TCGA Datasets

(A–D) (A) Receiver operating characteristic (ROC) curves shown for separating HPD patients from non-HPD patients in the validation dataset (Dataset_2, 21 HPD versus 30 non-HPD patients, AUC = 0.91 [95% CI, 0.87–0.96]); Kaplan-Meier analysis showed that the 121-gene set classifier can separate significantly low- and high-risk groups in all of the 13 major TCGA cancers, of which the top three cancers with greatest hazard ratios (HRs) were shown in (B) ESCA (HR = 100.1, 95% CI, 23.1–433.6); (C) COAD (HR = 17.5, 95% CI, 7.4–40.9), and (D) PAAD datasets (HR = 16.0, 95% CI, 8.8–29.0). See also Figures S9–S12.

network leading to suppression of the TP53 pathway activity. Previous studies showed that *KMT2C (MLL3)* co-activates *TP53*, whereas *KMT2C* levels decrease during cancer progression, which correlates with distinct clinical stages (Ford and Dingwall, 2015; Lee et al., 2009; Rabello et al., 2018). These results are consistent with our observations in HPD tumors after anti-PD-1 treatment.

Our RNA-seq data revealed that the IGF-1, ERK/MAPK, PI3K/AKT, and TGF-β signaling pathways were activated in the HPD tumors after anti-PD-1 therapy (Figure 3). Recent studies have found that TGF-β signaling may play an important role in resistance to immunotherapy. For example, Mariathasan et al. reported that lack of response to anti-PD-L1 antibody was associated with TGF-β signaling in fibroblasts and the exclusion of $CD8^+$ T cells, indicating that TGF-β-mediated stromal remodeling restricts T cell infiltration to

suppress antitumor immunity and that TGF-β inhibition may enhance the efficacy of immune checkpoint blockade (Mariathasan et al., 2018). In parallel, Tauriello et al. found that single-agent PD-1/PD-L1 inhibition had little effect, but co-targeting TGF-β produced a robust antitumor immune response that could prevent the development of metastasis and eliminate established metastases in a mouse model (Tauriello et al., 2018). Collectively, these studies indicate that inhibiting TGF-β could significantly improve the efficacy of anti-PD-1/anti-PD-L1 treatment (Mariathasan et al., 2018; Tauriello et al., 2018). Herein, our data suggest that enhanced TGF-β signaling could also contribute to the development of HPD after anti-PD-1 therapy. Therefore, inhibiting TGF-β signaling may also help prevent the development of HPD in response to anti-PD-1 treatment. Another interesting finding is the activation of PI3K/AKT in HPD tumors. A recent study demonstrated that the activity of PI3K/AKT signaling was crucial for lymphomas with PD-1 deletion (Wartewig et al., 2017). Therefore, when the tumors are exposed to anti-PD-1 therapy, elevated PI3K/AKT signaling may be another important mechanism for the survival, progression, or even hyperprogression of the tumor cells.

The HPD tumors had reduced tumor immunogenicity when compared with the pre-therapy tumors. Such reduction may be caused by downregulation of antigen-processing genes, including several *HLA* genes and *B2M*, and upregulation of certain immune checkpoint or modulator genes other than PD-1/PD-L1 (Figures 5 and 6). In the context of studying 28 immune cell populations critical to pan-cancer immunogenomics (Angelova et al., 2015; Charoentong et al., 2017), we found that the activity of eight immune cell populations were weakened and two were strengthened in the HPD tumors. The weakened immune cell populations including monocytes, CD4 helper T cells, dendritic cells, and NK cells may contribute to the ability of HPD tumors to escape immune surveillance. The enhanced cell populations such as neutrophils are known to have a number of pro-tumor properties (Galdiero et al., 2013; Mishalian et al., 2013; Sagiv et al., 2015; Tuting and de Visser, 2016), thus the increase in neutrophil activity in HPD tumors was not surprising.

The two patients developed HPD after anti-PD-1 therapy, indicating the adverse immunity changes that may result in an immunosuppressive environment. The decreased portion of immune cell phenotypes after anti-PD-1 therapy led us to speculate whether anti-PD-1 therapy contributed to accelerated AICD (activation-induced cell death) in these two patients. To test this hypothesis, we applied the GSVA approach to the apoptosis gene sets collected in the MSigDB database (Liberzon et al., 2015). It can be seen that five apoptosis gene sets were activated in the two patients after anti-PD-1 therapy (Figure S14A), of which 27 apoptotic genes including marker genes in caspase/bcl2 pathways (*CASP3*, *CASP7*, *BNIP2*, and *BNIP3L*) were significantly upregulated (Figure S14B). This indicated that the accelerated AICD may occur in the anti-tumor activating lymphocytes, which accounted for the decreased portion of immune cell phenotypes and enhanced immunosuppressive environment after anti-PD-1 therapy.

So far, cancer immunotherapies have largely focused on T lymphocytes. However, ILCs could also play important roles in the immune response. ILCs were classified into cytotoxic ILCs, such as NK cells, and helper-like ILCs, such as the ILC1, ILC2, and ILC3 subsets. Much of the role of ILCs other than NK cells in cancer and immunotherapy remain elusive. ILCs might represent promising targets in the context of cancer therapy because they are endowed with potent immunomodulatory properties. In the present study, we analyzed the dynamic changes in the activity of ILC populations associated with anti-PD-1 therapy. This represents the first study analyzing the ILC populations in hyperprogressive tumors after anti-PD-1 therapy. Although ILC1 and ILC2 subsets did not show significant changes according to GSEA (Figure S7), the ILC3 population was activated in HPD tumors compared with pre-therapy tumors (Figure 7). Among the three subsets of ILCs, the role of ILC3 is gaining increased interest for its potential tumor-promoting activities. ILC3 that produces interleukin (IL)-22 has also been shown to promote tumor growth mediated via STAT3 activation (Kirchberger et al., 2013). Another study showed that ILC3 promoted lymphatic metastasis by modulating the local chemokine milieu of cancer cells (Irshad et al., 2017). ILC3 may also promote tumor formation and progression by suppressing T cell responses (van Beek et al., 2016). It had been shown that intestinal ILC3 cells limit T cell responses and induce T cell death via outcompeting T cells for IL-2 (Hepworth et al., 2015). We observed upregulated expression of ILC3 marker genes by anti-PD-1 immunotherapy in the two HPD patients, which may contribute to the suppression of T cell responses or the induction of T cell death. Our findings were in line with those of previous studies, indicating that inhibiting ILC3 may complement anti-PD-1 treatment to reduce the likelihood of developing hyperprogressive tumors after the therapy.

It is worth mentioning that IL-22 expression was not detected in the before and after anti-PD-1 treatment FFPE samples of the two patients, which may be due to the influence of the degradation of the RNA samples from the FFPE specimens on gene expression study. However, previous studies have defined a large group of marker genes whose expressions were characteristic of the ILC3 cell population (Bjorklund et al., 2016; Wallrapp et al., 2017). For example, the ILC3 cells were defined by using a repertoire of around 400 genes (Bjorklund et al., 2016; Wallrapp et al., 2017), which became the basis of our analyses on ILC3 cells. Therefore, we analyzed the expression pattern changes of these marker genes to study the dynamic changes of ILC cell populations in response to the anti-PD-1 immunotherapy in the tumors of the HPD patients (Figures 7 and S7).

Previous research showed that PD-1-deficient mice were extraordinarily sensitive to tuberculosis and had much shorter survival times compared with wild-type mice (Lazar-Molnar et al., 2010). This sensitivity results from the need for the PD-1 pathway to control excessive inflammatory responses to tuberculosis infection in the lungs of mice (Lazar-Molnar et al., 2010). This led us to hypothesize that the PD-1 pathway may also be required to control excessive inflammatory responses in patients susceptible to HPD. If anti-PD-1 therapy is administered to HPD patients, it may contribute to tumor growth by further upregulating inflammatory pathway activities. The analyses of our data and those of others (Westin et al., 2014) confirmed this hypothesis by showing that anti-PD-1 therapy can further boost the pre-existing high levels of inflammation in HPD patients, and thus contribute to the hyperprogressive phenotype (Figures 8 and S8).

On the basis of genome-wide expression data of tumors from our study, and two publicly available datasets (before anti-PD-1 therapy) (Riaz et al., 2017; Westin et al., 2014), we identified and validated a 121-gene expression signature that can distinguish HPD patients from non-HPD patients. This may have significant clinical predictive value to identify patients who are suitable for anti-PD-1/anti-PD-L1 immunotherapy. Having validated this gene set, we examined whether there exists any mechanism that might explain its association with HPD. Interestingly, most of these genes (70 of 121) belonged to gene sets that we identified as significant to different aspects of the HPD tumors in our samples. Specifically, these genes could be classified into the following six categories that were described above as important contributors to the HPD phenotype (Figure S9): (1) somatic mutated gene sets; (2) oncogenic pathways of IGF-1, ERK/MAPK, PI3K/AKT, and TGF-β; (3) immune checkpoint genes; (4) ILC3 population marker genes; (5) marker genes for other immune populations like monocytes, CD4 T cells, and dendritic cells; and (6) differentially expressed genes in post-anti-PD-1 HPD tumors versus pre-anti-PD-1 non-HPD tumors. Thus, a significant portion of these HPD signature genes could be involved in the critical biological processes important to tumor evolution, infiltrated immune cells, and tumor-microenvironment interactions. However, although we validated the 121-gene set, more patient cohorts subjected to anti-PD-1 therapy that contain HPD and non-HPD patients are needed for prospective validation.

To better define HPD, especially to differentiate HPD from intermediate and/or late tumor progression, we compared the mutational and gene expression of the two original samples in our study with the pre-treatment tumor samples of the four patients (#28, #9, #26, #38) who developed intermediate and/or late tumor progression (Table S6). Mutation analysis showed that 40 cancer genes had nonsilent somatic mutations in the original tumors of the HPD patients but no mutations in the tumors of the patients whose tumor progression was intermediate and/or late (Figure S15). These genes include, for example, *MUC13*, *MUC6*, *APC2*, *ARID2*, *CDK4*, *EP400*, *MARK4*, *MDM4*, *MUC2*, *NOTCH1*, and *SLIT2*. Previous research demonstrated that *MDM4* alteration was significantly associated with hyperprogression in patients subjected to immunotherapy (Kato et al., 2017), which was consistent with our results. We tabulated the information of these 40 HPD-associated cancer genes in Table S7. At the transcriptome level, GSVA identified four gene sets from the MsigDB database that were significantly altered in the tumors of HPD patients compared with the patients with intermediate and/or late tumor progression. These gene sets were: HALLMARK_REACTIVE_OXIGEN_SPECIES_PATHWAY, HALLMARK_DNA_REPAIR, HALLMARK_ADIPOGENESIS, and SINGH_KRAS_DEPENDENCY_SIGNATURE. The first three pathways, i.e., the reactive oxygen species pathway, the DNA repair pathway, and the adipogenesis pathway, were significantly inhibited, whereas the KRAS signaling pathway was significantly activated in the tumors of HPD patients relative to the patients with intermediate and/or late tumor progression (Figure S16A). The corresponding gene expression changes of the above significantly altered pathways were also shown (Figure S16B). Together, these mutational and transcriptional changes of the tumors between the HPD and the intermediate/late tumor progression patients may contribute to the better characterization of the HPD condition.

Overall, our comprehensive analysis of HPD tumors after anti-PD-1 therapy and pre-therapy tumors identified the genomics and immune factors contributing to the hyperprogression phenotypes, such as deleterious somatic mutations in important tumor suppressors such as *TSC2* and *VHL*, downregulated antigen-processing genes, and upregulated immune checkpoints or modulators other than PD-1/PD-L1. We also identified immune cell populations with significant activity changes in the HPD tumors; particularly the ILC subset, ILC3, was found to be activated in the HPD tumors after anti-PD-1 treatment. A gene expression signature for HPD tumors was also identified and validated using our samples and publicly available datasets. Our findings may contribute to understanding the mechanisms of the development of HPD after anti-PD-1 treatment, which is important to identify patients at high risk of developing HPD.

Limitations of Study

In this study, we analyzed the genomics, transcriptomics, and immunogenicity of two patients subjected to anti-PD-1 immunotherapy who developed hyperprogression after the treatment. We acknowledged that the patient sample size was small in this study. This is because the majority of the patients either did not develop hyperprogression or had the pseudo-hyperprogressive phenotype after checkpoint immunotherapy. Further larger patient samples involving more HPD patients treated with anti-PD-1 are needed to validate and extend our findings. Another limitation is that we only profiled HPD tumor sample one time upon hyperprogression after anti-PD-1 immunotherapy and did not collect post-hyperprogression tumor samples at later time points. This design rendered us unable to investigate whether the associated immunosuppressive profiles of HPD tumors remain as such even at later time points. However, our study is innovative in terms of analyzing both the before- and after-immunotherapy DNA/RNA samples of the HPD patients and serves as the starting point for similar studies that are lacking in the field.

Currently, the two outside datasets we used in the manuscript were the only ones that have the transcriptome-level gene expression data available publicly for us to develop a gene expression profile for HPD (Riaz et al., 2017; Westin et al., 2014). Based on the available data, we characterized a 121-gene expression profile to differentiate HPD patients from non-HPD patients in both the datasets (Riaz et al., 2017; Westin et al., 2014) with high AUC values and high sensitivity and specificity as described in the manuscript. More HPD patients with well-profiled transcriptome data and detailed clinical information related to the anti-PD-1 treatment are needed to verify our gene expression signature.

METHODS

All methods can be found in the accompanying Transparent Methods supplemental file.

DATA AND SOFTWARE AVAILABILITY

The WES and RNA-seq raw sequence reads data from the before and after anti-PD-1 immunotherapy FFPE samples from the two cancer patients (4 FFPE samples) have been deposited in the Sequence Read Archive under accession number of PRJNA503522.

SUPPLEMENTAL INFORMATION

Supplemental Information includes Transparent Methods, 16 figures, and 7 tables and can be found with this article online at https://doi.org/10.1016/j.isci.2018.10.021.

ACKNOWLEDGMENTS

We thank the outside reviewers for manuscript suggestions and revisions. This work was supported by NIH grants N01CN201200015 and R01CA134682.

AUTHOR CONTRIBUTIONS

M.Y. and Y.W. conceived the project and revised the manuscript. D.X. performed the experiment and all the data analyses and writing of the paper. A.K.S and A.C.M collected the samples for this study. B.G. recruited the patients and revised the manuscript.

DECLARATION OF INTERESTS

The authors declare no competing interests.

Received: June 29, 2018
Revised: September 14, 2018
Accepted: October 19, 2018
Published: November 30, 2018

REFERENCES

Angelova, M., Charoentong, P., Hackl, H., Fischer, M.L., Snajder, R., Krogsdam, A.M., Waldner, M.J., Bindea, G., Mlecnik, B., Galon, J., et al. (2015). Characterization of the immunophenotypes and antigenomes of colorectal cancers reveals distinct tumor escape mechanisms and novel targets for immunotherapy. Genome Biol. *16*, 64.

Biton, J., Mansuet-Lupo, A., Pecuchet, N., Alifano, M., Ouakrim, H., Arrondeau, J., Boudou-Rouquette, P., Goldwasser, F., Leroy, K., Goc, J., et al. (2018). TP53, STK11 and EGFR mutations predict tumor immune profile and the response to anti-PD-1 in lung adenocarcinoma. Clin. Cancer Res. *9*, 1–14.

Bjorklund, A.K., Forkel, M., Picelli, S., Konya, V., Theorell, J., Friberg, D., Sandberg, R., and Mjosberg, J. (2016). The heterogeneity of human CD127(+) innate lymphoid cells revealed by single-cell RNA sequencing. Nat. Immunol. *17*, 451–460.

Cerami, E., Gao, J., Dogrusoz, U., Gross, B.E., Sumer, S.O., Aksoy, B.A., Jacobsen, A., Byrne, C.J., Heuer, M.L., Larsson, E., et al. (2012). The cBio cancer genomics portal: an open platform for exploring multidimensional cancer genomics data. Cancer Discov. *2*, 401–404.

Champiat, S., Dercle, L., Ammari, S., Massard, C., Hollebecque, A., Postel-Vinay, S., Chaput, N., Eggermont, A., Marabelle, A., Soria, J.C., et al. (2017). Hyperprogressive disease is a new pattern of progression in cancer patients treated by anti-PD-1/PD-L1. Clin. Cancer Res. *23*, 1920–1928.

Charoentong, P., Finotello, F., Angelova, M., Mayer, C., Efremova, M., Rieder, D., Hackl, H., and Trajanoski, Z. (2017). Pan-cancer immunogenomic analyses reveal genotype-immunophenotype relationships and predictors of response to checkpoint blockade. Cell Rep. *18*, 248–262.

Dang, H.X., White, B.S., Foltz, S.M., Miller, C.A., Luo, J., Fields, R.C., and Maher, C.A. (2017). ClonEvol: clonal ordering and visualization in cancer sequencing. Ann. Oncol. *28*, 3076–3082.

Ford, D.J., and Dingwall, A.K. (2015). The cancer COMPASS: navigating the functions of MLL complexes in cancer. Cancer Genet. *208*, 178–191.

Fung, K.Y., Nguyen, P.M., and Putoczki, T. (2017). The expanding role of innate lymphoid cells and their T-cell counterparts in gastrointestinal cancers. Mol. Immunol. *11*, 1–9.

Galdiero, M.R., Bonavita, E., Barajon, I., Garlanda, C., Mantovani, A., and Jaillon, S. (2013). Tumor associated macrophages and neutrophils in cancer. Immunobiology *218*, 1402–1410.

Gao, J., Aksoy, B.A., Dogrusoz, U., Dresdner, G., Gross, B., Sumer, S.O., Sun, Y., Jacobsen, A., Sinha, R., Larsson, E., et al. (2013). Integrative analysis of complex cancer genomics and clinical profiles using the cBioPortal. Sci. Signal. *6*, pl1.

Goncharova, E., Goncharov, D., Noonan, D., and Krymskaya, V.P. (2004). TSC2 modulates actin cytoskeleton and focal adhesion through TSC1-binding domain and the Rac1 GTPase. J. Cell Biol. *167*, 1171–1182.

Goncharova, E.A., Goncharov, D.A., Lim, P.N., Noonan, D., and Krymskaya, V.P. (2006). Modulation of cell migration and invasiveness by tumor suppressor TSC2 in lymphangioleiomyomatosis. Am. J. Respir. Cell Mol. Biol. *34*, 473–480.

Gong, J., Wang, C., Lee, P.P., Chu, P., and Fakih, M. (2017). Response to PD-1 blockade in microsatellite stable metastatic colorectal cancer harboring a POLE mutation. J. Natl. Compr. Canc Netw. *15*, 142–147.

Gossage, L., Eisen, T., and Maher, E.R. (2015). VHL, the story of a tumour suppressor gene. Nat. Rev. Cancer *15*, 55–64.

Hanna, G.J., Lizotte, P., Cavanaugh, M., Kuo, F.C., Shivdasani, P., Frieden, A., Chau, N.G., Schoenfeld, J.D., Lorch, J.H., Uppaluri, R., et al. (2018). Frameshift events predict anti-PD-1/L1 response in head and neck cancer. JCI Insight *3*, 1–13.

Hanzelmann, S., Castelo, R., and Guinney, J. (2013). GSVA: gene set variation analysis for microarray and RNA-seq data. BMC Bioinformatics *14*, 7.

Hepworth, M.R., Fung, T.C., Masur, S.H., Kelsen, J.R., McConnell, F.M., Dubrot, J., Withers, D.R., Hugues, S., Farrar, M.A., Reith, W., et al. (2015). Immune tolerance. Group 3 innate lymphoid cells mediate intestinal selection of commensal bacteria-specific CD4(+) T cells. Science *348*, 1031–1035.

Hugo, W., Zaretsky, J.M., Sun, L., Song, C., Moreno, B.H., Hu-Lieskovan, S., Berent-Maoz, B., Pang, J., Chmielowski, B., Cherry, G., et al. (2016). Genomic and transcriptomic features of response to anti-PD-1 therapy in metastatic melanoma. Cell *165*, 35–44.

Irshad, S., Flores-Borja, F., Lawler, K., Monypenny, J., Evans, R., Male, V., Gordon, P., Cheung, A., Gazinska, P., Noor, F., et al. (2017). RORgammat(+) innate lymphoid cells promote lymph node metastasis of breast cancers. Cancer Res. *77*, 1083–1096.

Kammerer-Jacquet, S.F., Crouzet, L., Brunot, A., Dagher, J., Pladys, A., Edeline, J., Laguerre, B., Peyronnet, B., Mathieu, R., Verhoest, G., et al. (2017). Independent association of PD-L1 expression with noninactivated VHL clear cell renal cell carcinoma-A finding with therapeutic potential. Int. J. Cancer *140*, 142–148.

Kato, S., Goodman, A., Walavalkar, V., Barkauskas, D.A., Sharabi, A., and Kurzrock, R. (2017). Hyperprogressors after immunotherapy: analysis of genomic alterations associated with accelerated growth rate. Clin. Cancer Res. *23*, 4242–4250.

Kirchberger, S., Royston, D.J., Boulard, O., Thornton, E., Franchini, F., Szabady, R.L., Harrison, O., and Powrie, F. (2013). Innate lymphoid cells sustain colon cancer through production of interleukin-22 in a mouse model. J. Exp. Med. *210*, 917–931.

Koyama, S., Akbay, E.A., Li, Y.Y., Herter-Sprie, G.S., Buczkowski, K.A., Richards, W.G., Gandhi, L., Redig, A.J., Rodig, S.J., Asahina, H., et al. (2016). Adaptive resistance to therapeutic PD-1 blockade is associated with upregulation of alternative immune checkpoints. Nat. Commun. *7*, 10501.

Lazar-Molnar, E., Chen, B., Sweeney, K.A., Wang, E.J., Liu, W., Lin, J., Porcelli, S.A., Almo, S.C., Nathenson, S.G., and Jacobs, W.R., Jr. (2010). Programmed death-1 (PD-1)-deficient mice are extraordinarily sensitive to tuberculosis. Proc. Natl. Acad. Sci. U S A *107*, 13402–13407.

Lee, J., Kim, D.H., Lee, S., Yang, Q.H., Lee, D.K., Lee, S.K., Roeder, R.G., and Lee, J.W. (2009). A tumor suppressive coactivator complex of p53 containing ASC-2 and histone H3-lysine-4 methyltransferase MLL3 or its paralogue MLL4. Proc. Natl. Acad. Sci. U S A *106*, 8513–8518.

Liberzon, A., Birger, C., Thorvaldsdottir, H., Ghandi, M., Mesirov, J.P., and Tamayo, P. (2015). The molecular signatures database (MSigDB) hallmark gene set collection. Cell Syst. *1*, 417–425.

Liberzon, A., Subramanian, A., Pinchback, R., Thorvaldsdottir, H., Tamayo, P., and Mesirov, J.P. (2011). Molecular signatures database (MSigDB) 3.0. Bioinformatics *27*, 1739–1740.

Mariathasan, S., Turley, S.J., Nickles, D., Castiglioni, A., Yuen, K., Wang, Y., Kadel, E.E., III, Koeppen, H., Astarita, J.L., Cubas, R., et al. (2018). TGFbeta attenuates tumour response to PD-L1 blockade by contributing to exclusion of T cells. Nature *554*, 544–548.

Menon, S., Dibble, C.C., Talbott, G., Hoxhaj, G., Valvezan, A.J., Takahashi, H., Cantley, L.C., and Manning, B.D. (2014). Spatial control of the TSC complex integrates insulin and nutrient regulation of mTORC1 at the lysosome. Cell *156*, 771–785.

Miao, D., Margolis, C.A., Gao, W., Voss, M.H., Li, W., Martini, D.J., Norton, C., Bosse, D., Wankowicz, S.M., Cullen, D., et al. (2018). Genomic correlates of response to immune checkpoint therapies in clear cell renal cell carcinoma. Science *359*, 801–806.

Mishalian, I., Bayuh, R., Levy, L., Zolotarov, L., Michaeli, J., and Fridlender, Z.G. (2013). Tumor-associated neutrophils (TAN) develop pro-tumorigenic properties during tumor progression. Cancer Immunol. Immunother. *62*, 1745–1756.

Niknafs, N., Kim, D., Kim, R., Diekhans, M., Ryan, M., Stenson, P.D., Cooper, D.N., and Karchin, R. (2013). MuPIT interactive: webserver for mapping variant positions to annotated, interactive 3D structures. Hum. Genet. *132*, 1235–1243.

Rabello, D.D.A., Ferreira, V., Berzoti-Coelho, M.G., Burin, S.M., Magro, C.L., Cacemiro, M.D.C., Simoes, B.P., Saldanha-Araujo, F., de Castro, F.A., and Pittella-Silva, F. (2018). MLL2/KMT2D and MLL3/KMT2C expression correlates with disease progression and response to imatinib mesylate in chronic myeloid leukemia. Cancer Cell Int. *18*, 26.

Riaz, N., Havel, J.J., Makarov, V., Desrichard, A., Urba, W.J., Sims, J.S., Hodi, F.S., Martin-Algarra, S., Mandal, R., Sharfman, W.H., et al. (2017). Tumor and microenvironment evolution during immunotherapy with Nivolumab. Cell *171*, 934–949.e15.

Rizvi, N.A., Hellmann, M.D., Snyder, A., Kvistborg, P., Makarov, V., Havel, J.J., Lee, W., Yuan, J., Wong, P., Ho, T.S., et al. (2015). Cancer immunology. Mutational landscape determines sensitivity to PD-1 blockade in non-small cell lung cancer. Science *348*, 124–128.

Saada-Bouzid, E., Defaucheux, C., Karabajakian, A., Coloma, V.P., Servois, V., Paoletti, X., Even, C., Fayette, J., Guigay, J., Loirat, D., et al. (2017). Hyperprogression during anti-PD-1/PD-L1 therapy in patients with recurrent and/or metastatic head and neck squamous cell carcinoma. Ann. Oncol. *28*, 1605–1611.

Sagiv, J.Y., Michaeli, J., Assi, S., Mishalian, I., Kisos, H., Levy, L., Damti, P., Lumbroso, D., Polyansky, L., Sionov, R.V., et al. (2015). Phenotypic diversity and plasticity in circulating neutrophil subpopulations in cancer. Cell Rep. *10*, 562–573.

Sharma, P., and Allison, J.P. (2015). Immune checkpoint targeting in cancer therapy: toward combination strategies with curative potential. Cell *161*, 205–214.

Sharma, P., Hu-Lieskovan, S., Wargo, J.A., and Ribas, A. (2017). Primary, adaptive, and acquired resistance to cancer immunotherapy. Cell *168*, 707–723.

Spits, H., Artis, D., Colonna, M., Diefenbach, A., Di Santo, J.P., Eberl, G., Koyasu, S., Locksley, R.M., McKenzie, A.N., Mebius, R.E., et al. (2013). Innate lymphoid cells–a proposal for uniform nomenclature. Nat. Rev. Immunol. *13*, 145–149.

Subramanian, A., Tamayo, P., Mootha, V.K., Mukherjee, S., Ebert, B.L., Gillette, M.A., Paulovich, A., Pomeroy, S.L., Golub, T.R., Lander, E.S., et al. (2005). Gene set enrichment analysis: a knowledge-based approach for interpreting genome-wide expression profiles. Proc. Natl. Acad. Sci. U S A *102*, 15545–15550.

Tauriello, D.V.F., Palomo-Ponce, S., Stork, D., Berenguer-Llergo, A., Badia-Ramentol, J., Iglesias, M., Sevillano, M., Ibiza, S., Canellas, A., Hernando-Momblona, X., et al. (2018). TGFbeta drives immune evasion in genetically reconstituted colon cancer metastasis. Nature *554*, 538–543.

Teo, M.Y., Seier, K., Ostrovnaya, I., Regazzi, A.M., Kania, B.E., Moran, M.M., Cipolla, C.K., Bluth, M.J., Chaim, J., Al-Ahmadie, H., et al. (2018). Alterations in DNA damage response and repair genes as potential marker of clinical benefit from PD-1/PD-L1 blockade in advanced urothelial cancers. J. Clin. Oncol. *36*, 1685–1694.

Topalian, S.L., Drake, C.G., and Pardoll, D.M. (2012). Targeting the PD-1/B7-H1(PD-L1) pathway to activate anti-tumor immunity. Curr. Opin. Immunol. *24*, 207–212.

Tuting, T., and de Visser, K.E. (2016). CANCER. How neutrophils promote metastasis. Science *352*, 145–146.

van Beek, J.J.P., Martens, A.W.J., Bakdash, G., and de Vries, I.J.M. (2016). Innate lymphoid cells in tumor immunity. Biomedicines *4*, 7–21.

Wallrapp, A., Riesenfeld, S.J., Burkett, P.R., Abdulnour, R.E., Nyman, J., Dionne, D., Hofree, M., Cuoco, M.S., Rodman, C., Farouq, D., et al. (2017). The neuropeptide NMU amplifies ILC2-driven allergic lung inflammation. Nature *549*, 351–356.

Wartewig, T., Kurgyis, Z., Keppler, S., Pechloff, K., Hameister, E., Ollinger, R., Maresch, R., Buch, T., Steiger, K., Winter, C., et al. (2017). PD-1 is a haploinsufficient suppressor of T cell lymphomagenesis. Nature *552*, 121–125.

Westin, J.R., Chu, F., Zhang, M., Fayad, L.E., Kwak, L.W., Fowler, N., Romaguera, J., Hagemeister, F., Fanale, M., Samaniego, F., et al. (2014). Safety and activity of PD1 blockade by pidilizumab in combination with rituximab in patients with relapsed follicular lymphoma: a single group, open-label, phase 2 trial. Lancet Oncol. *15*, 69–77.

Yoshikawa, S., Kiyohara, Y., Otsuka, M., Kondou, R., Nonomura, C., Miyata, H., Iizuka, A., Ohshima, K., Urakami, K., Nagashima, T., et al. (2017). Multi-omics profiling of patients with melanoma treated with Nivolumab in project HOPE. Anticancer Res. *37*, 1321–1328.

Zaretsky, J.M., Garcia-Diaz, A., Shin, D.S., Escuin-Ordinas, H., Hugo, W., Hu-Lieskovan, S., Torrejon, D.Y., Abril-Rodriguez, G., Sandoval, S., Barthly, L., et al. (2016). Mutations associated with acquired resistance to PD-1 blockade in melanoma. N. Engl. J. Med. *375*, 819–829.

Zhang, J., Xu, X., Shi, M., Chen, Y., Yu, D., Zhao, C., Gu, Y., Yang, B., Guo, S., Ding, G., et al. (2017). CD13(hi) Neutrophil-like myeloid-derived suppressor cells exert immune suppression through Arginase 1 expression in pancreatic ductal adenocarcinoma. Oncoimmunology *6*, e1258504.

Zoncu, R., Efeyan, A., and Sabatini, D.M. (2011). mTOR: from growth signal integration to cancer, diabetes and ageing. Nat. Rev. Mol. Cell Biol. *12*, 21–35.

ISCI, Volume *9*

Supplemental Information

Immunogenomic Landscape Contributes to Hyperprogressive Disease after Anti-PD-1 Immunotherapy for Cancer

Donghai Xiong, Yian Wang, Arun K. Singavi, Alexander C. Mackinnon, Ben George, and Ming You

Supplemental Information

A

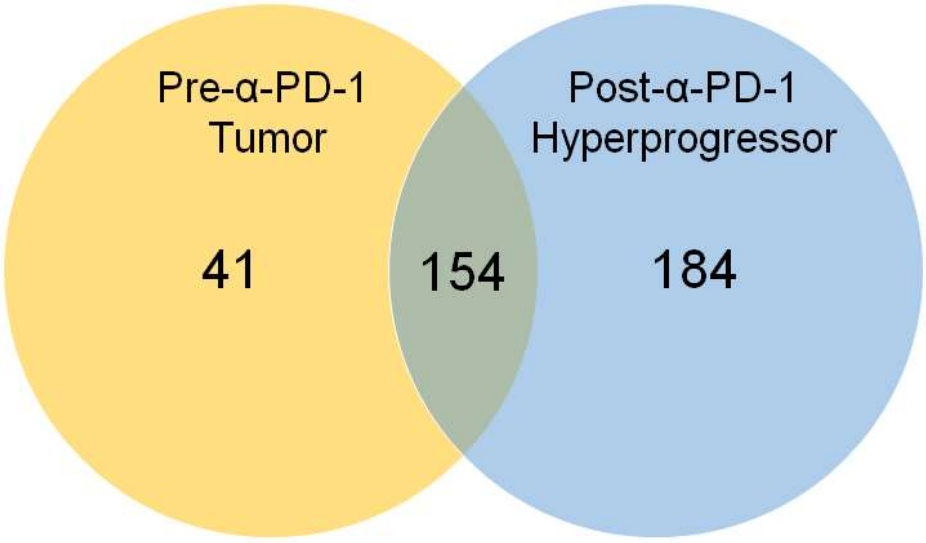

B

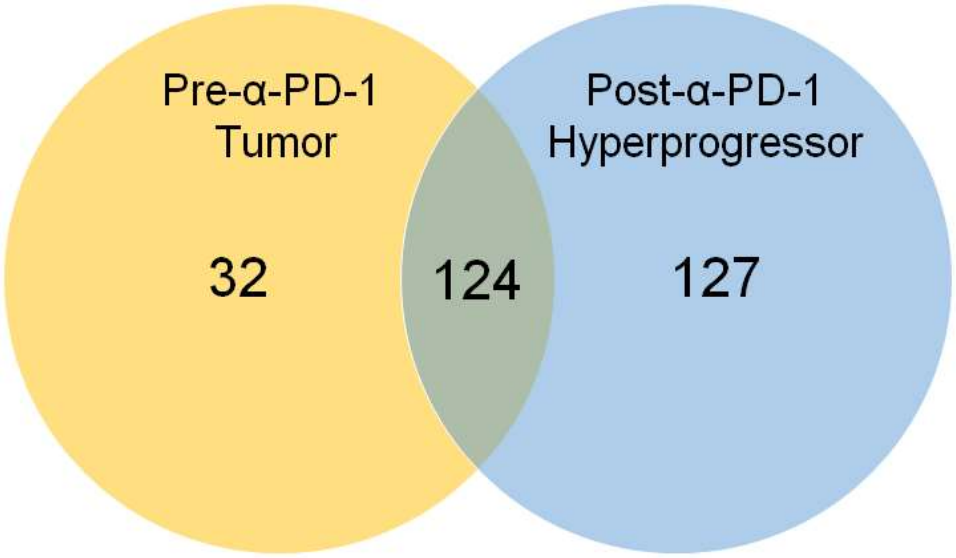

Figure S1. The number of somatic mutations in the pre- and post- anti-PD-1 treatment tumor samples of the two patients. Related to Figure 1 and Figure 2. A) Patient 1; B) Patient 2.

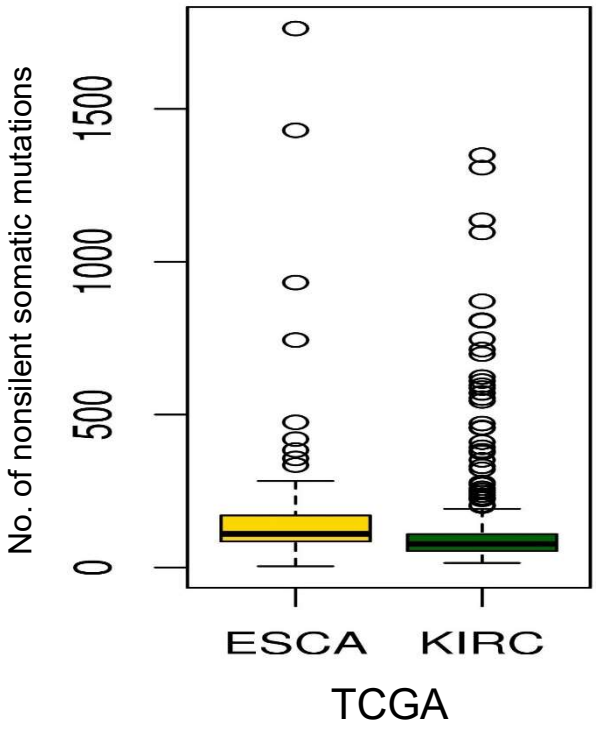

Figure S2. The distribution of nonsilent somatic mutations in the two TCGA cancer types anaylzed in the hyperprogressive tumor context in the present study. Related to Figure 1 and Figure 2. The numbers of nonsilent somatic mutations of the esophageal carcinoma (ESCA, n=184) and kidney renal clear cell carcinoma (KIRC, n=384) samples from TCGA.

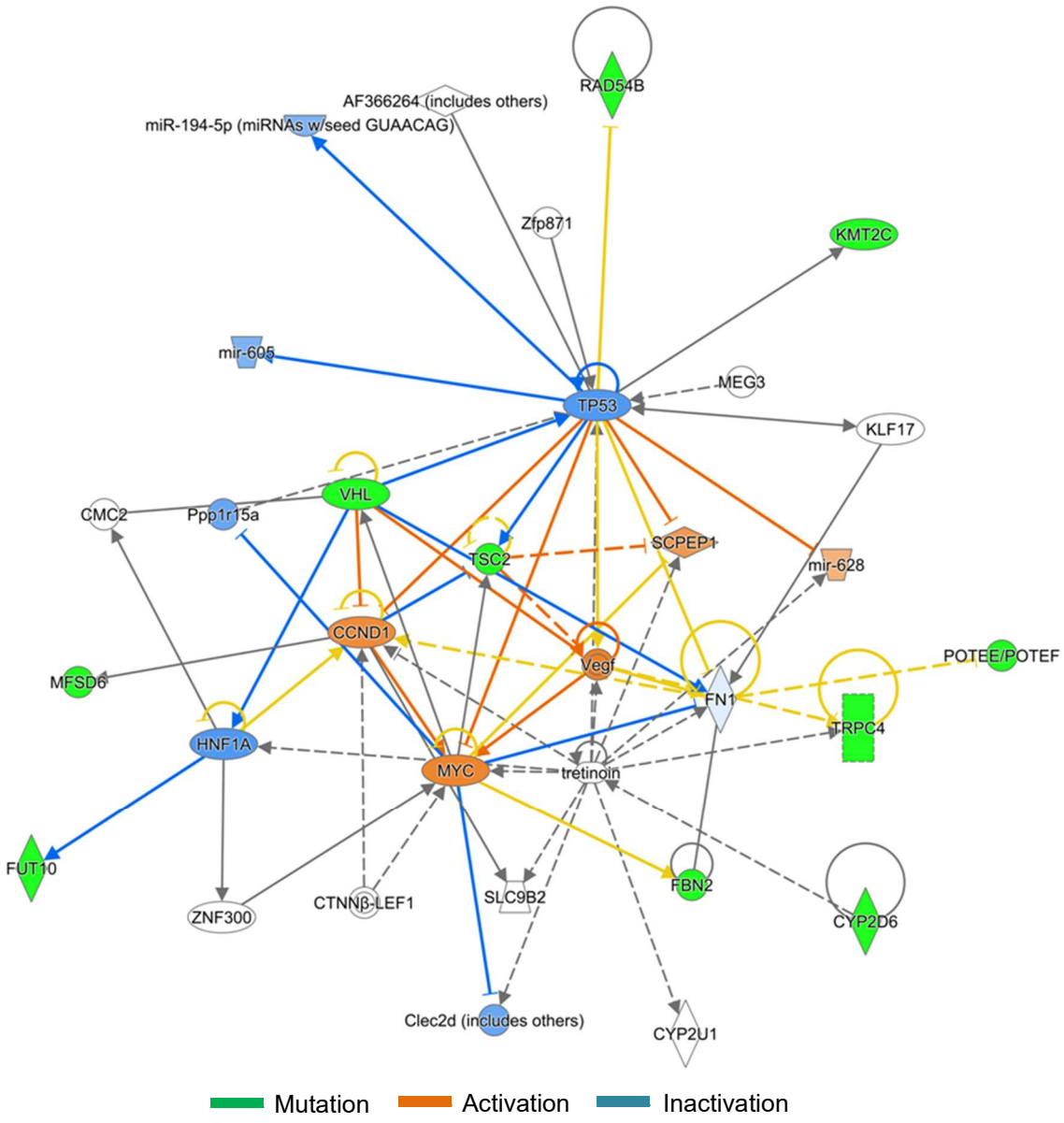

Figure S3. Key mutated cancer genes interacting network. Related to Table 2. Based on the eleven genes with the deleterious somatic mutations, a mechanistic network was built by IPA in which ten genes carrying these mutations resulted in the suppression of TP53 tumor suppressor pathway and activation of MYC, CCND1 and VEGF oncogenic pathways.

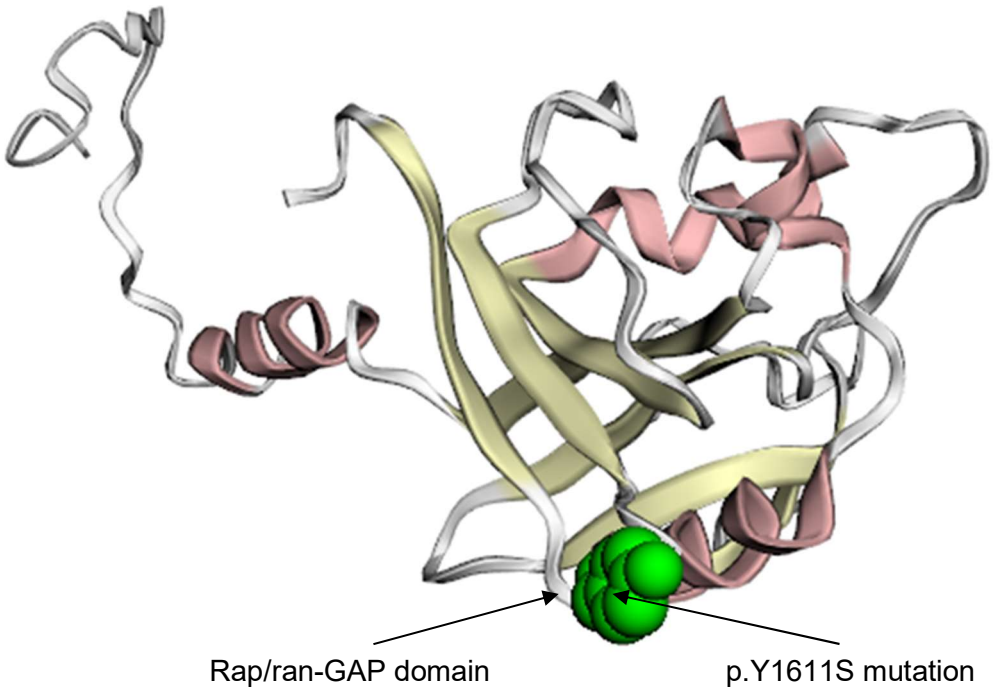

Figure S4. Key mutation in the TSC2 protein. Related to Table 2. The 3D structure of the TSC2 protein and the location of the amino acid residue harboring the p.Y1611S mutation, which is within the Rap/ran-GAP domain of the TSC2 protein critical to its biological function.

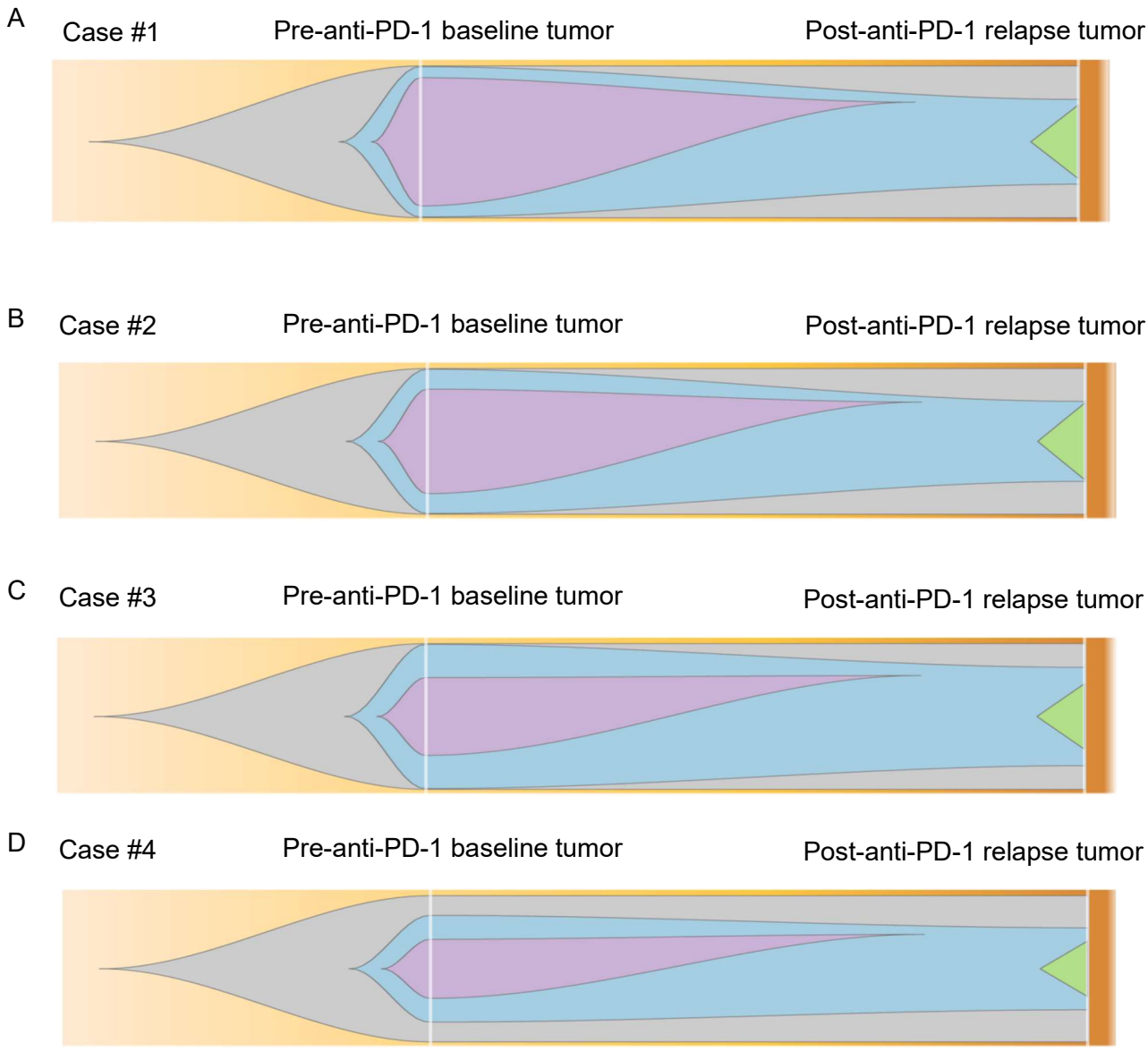

Figure S5. Clonal evolution from the pre-anti-PD1 therapy baseline tumor to post-anti-PD-1 relapsing tumor in the four melanoma patients from a previous study. Related to Figure 4. The graphical representation of clonal evolution in the four melanoma patients: (A) Case #1; (B) Case #2; (C) Case #3; (D) Case #4.

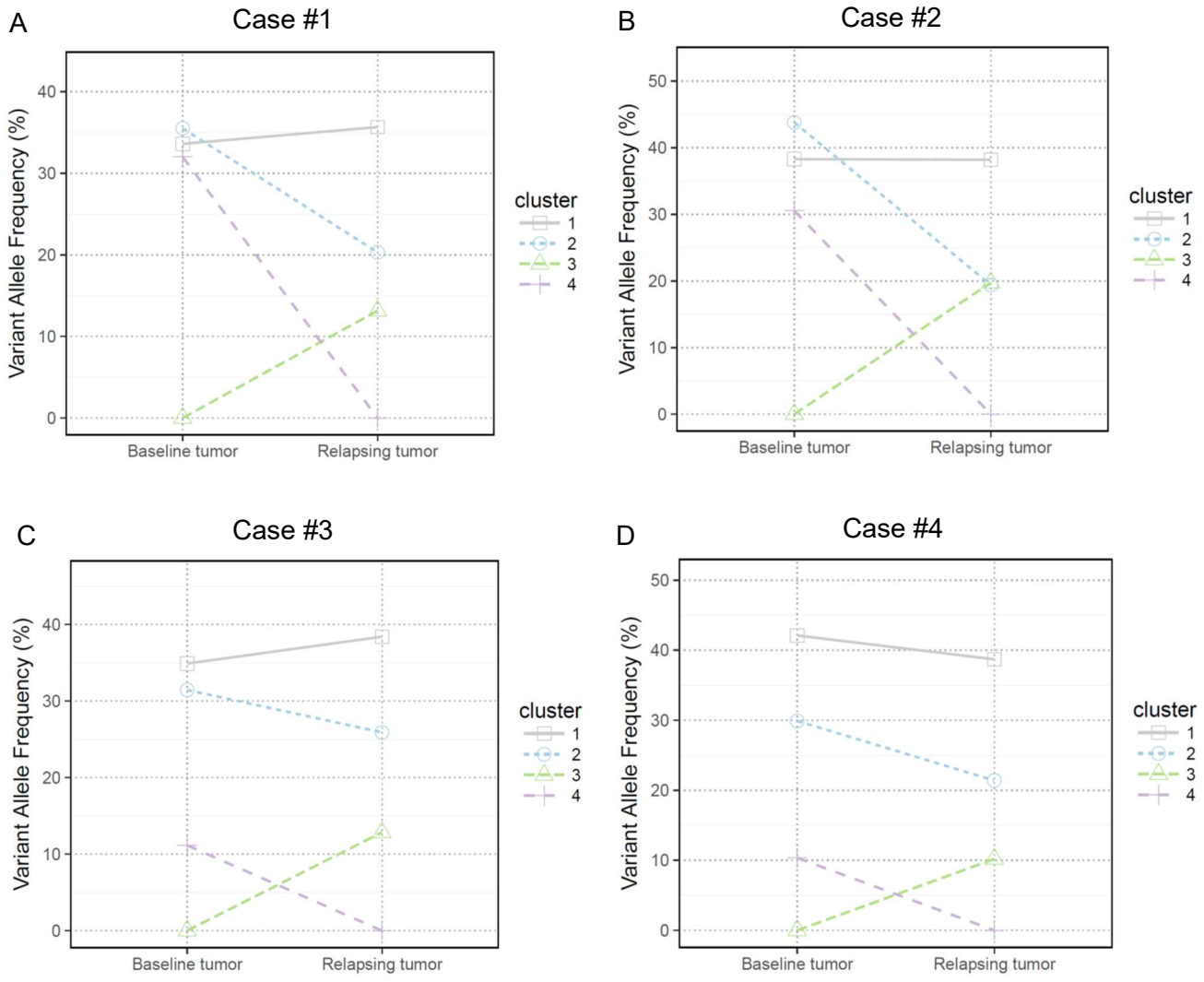

Figure S6. The mutation clusters representing clonal evolution from the pre-anti-PD1 therapy baseline tumor to post-anti-PD-1 relapsing tumor in the four melanoma patients from a previous study. Related to Figure 4. The mutation clusters detected in the pre-anti-PD1 therapy baseline tumor to post-anti-PD-1 relapsing tumor in the patients: (A) Case #1; (B) Case #2; (C) Case #3; (D) Case #4. The relationship between the clusters in the pre-therapy and post-therapy tumors are indicated by lines linking them.

A. ILC1 population

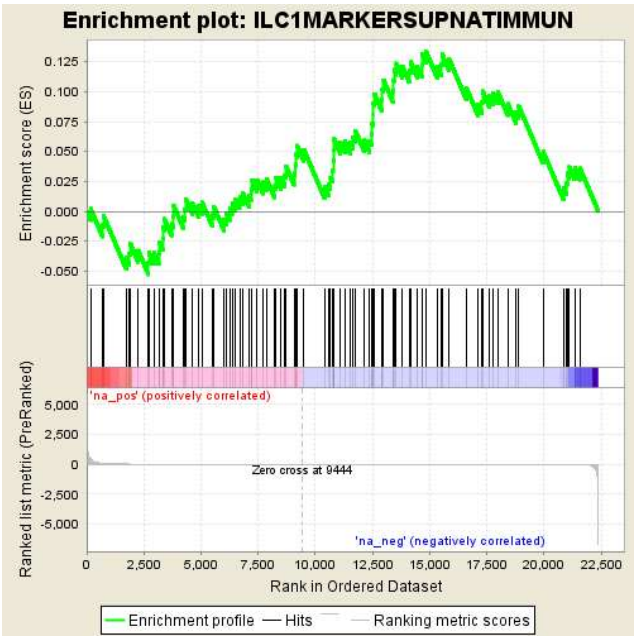

B. ILC2 population

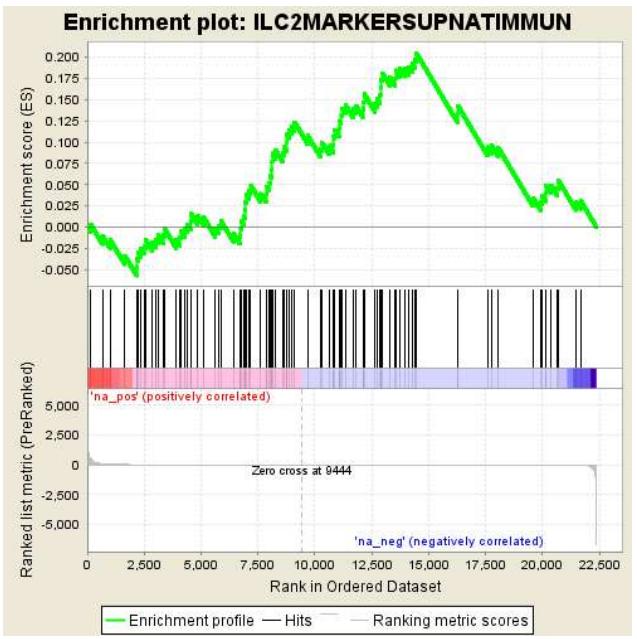

Figure S7. The ILC1 and ILC2 populations activity do not have significant changes in the HPD tumors after anti-PD-1 therapy. Related to Figure 7. (A) The ILC1 and (B) the ILC2 marker genes were not enriched in either the top up- or down-regulated genes in the HPD tumors.

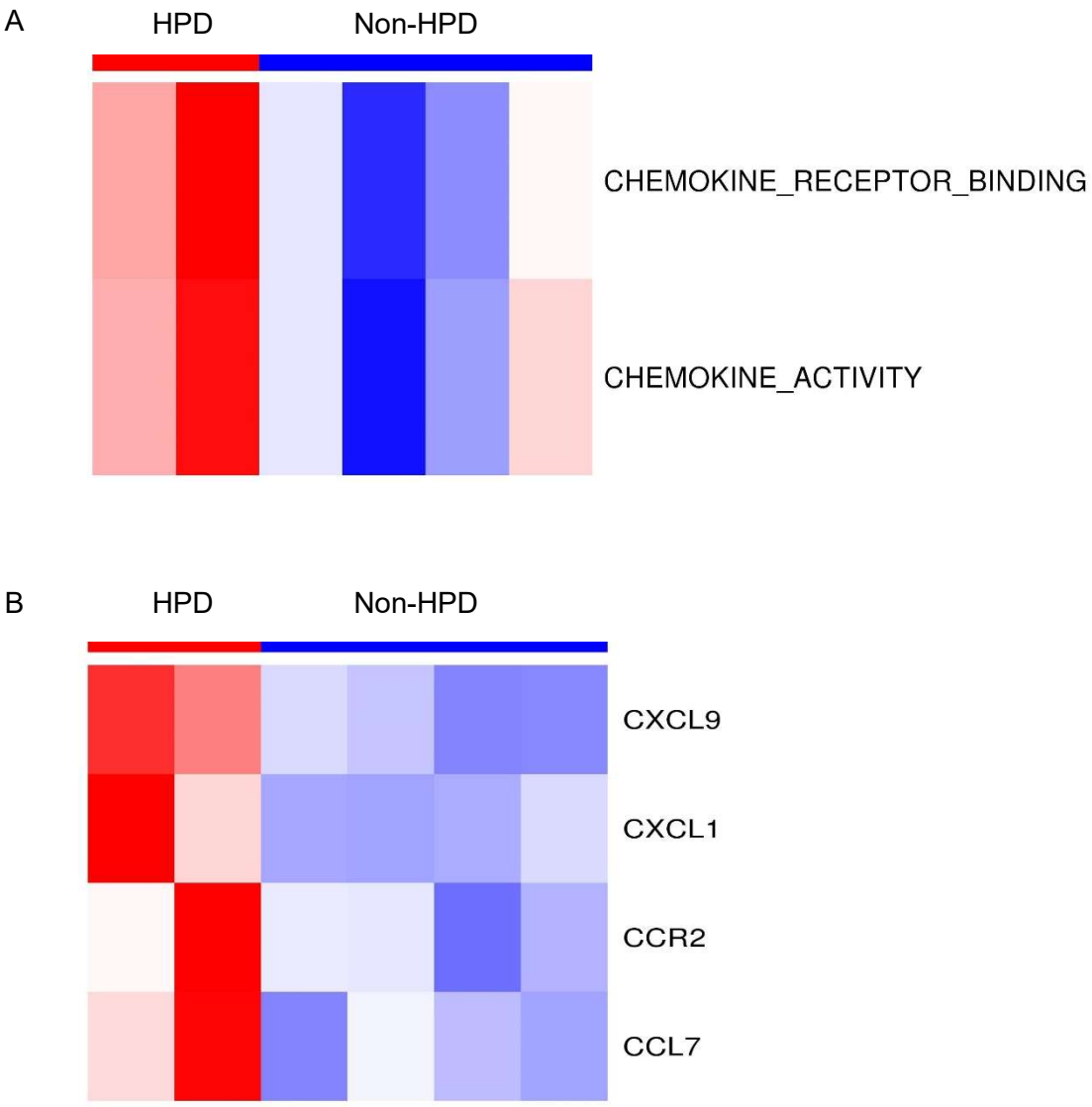

Figure S8. Pre-α-PD-1 therapy tumors of hyperprogressive patients have elevated inflammation pathway activity (mainly chemokine activity) compared to the responsive patients. Related to Figure 8. (A) GSVA identified the activation of two founder data sets of inflammation pathways in the pre-therapy tumors of HPD patients compared to the non-HPD patients; (B) The chemokine encoding genes that were up-regulated in the pre-therapy tumors of HPD patients compared to the non-HPD patients.

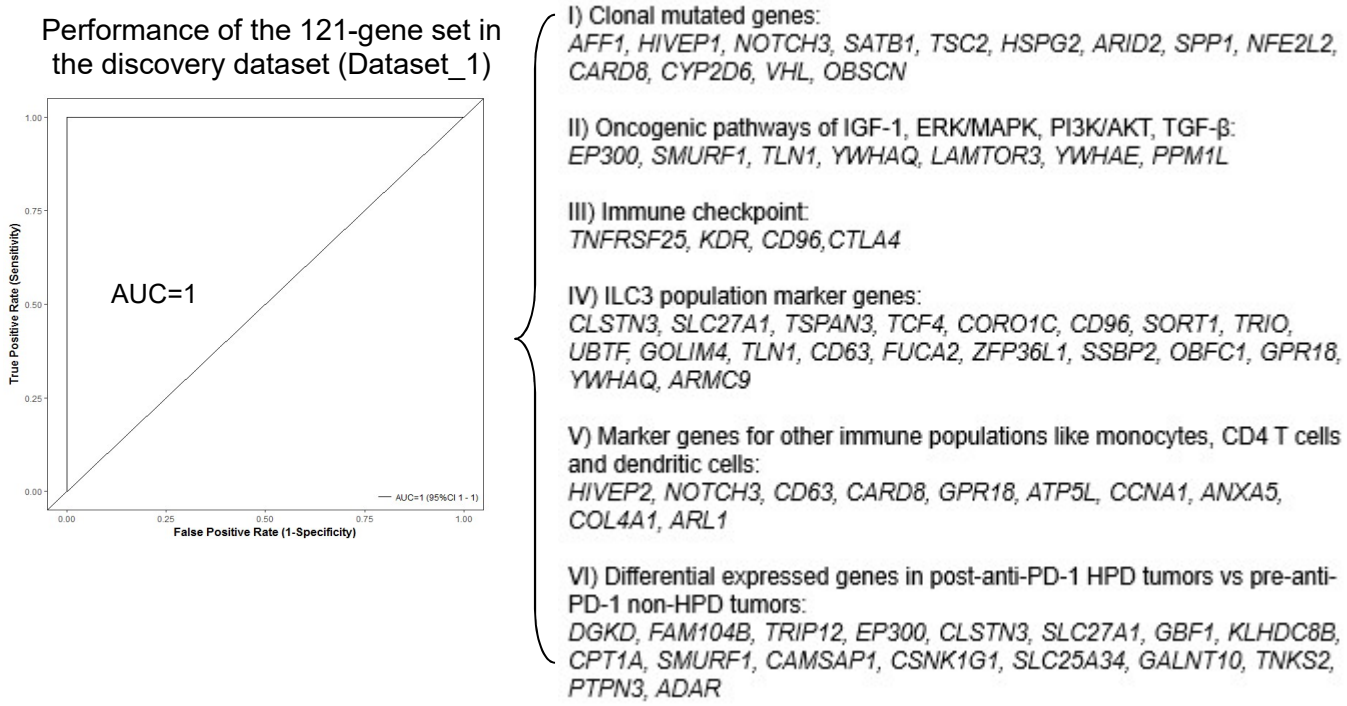

Figure S9. Results of the 121-gene expression signature in the discovery data set (Dataset_1). Related to Figure 9. ROC curves was shown for separating HPD patients from non-HPD patients in the discovery data set (4 HPD vs 16 non-HPD patients, AUC=1). The majority of these genes (70 of 121) belonged to the gene sets that we identified as significant to different aspects of the HPD tumors in our samples. Specifically, these genes were classified into the following six categories.

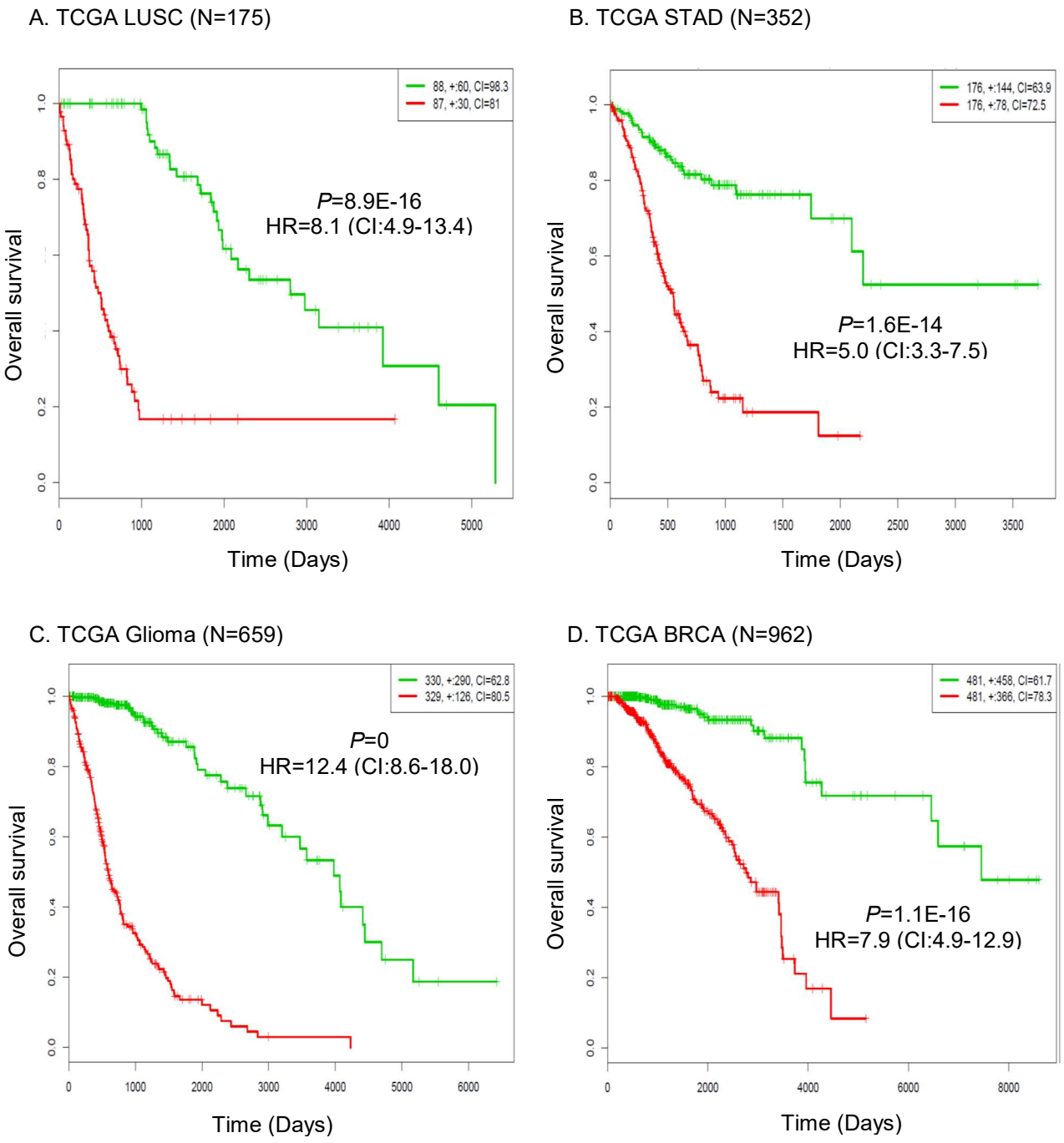

Figure S10. Kaplan–Meier analysis showed that the 121-gene set classifier can separate significantly low- and high-risk groups in the 13 major TCGA cancers. Related to Figure 9. The Kaplan–Meier curves of the TCGA cancer types of (A) LUSC, (B) STAD, (C) glioma, (D) BRCA were shown in this figure.

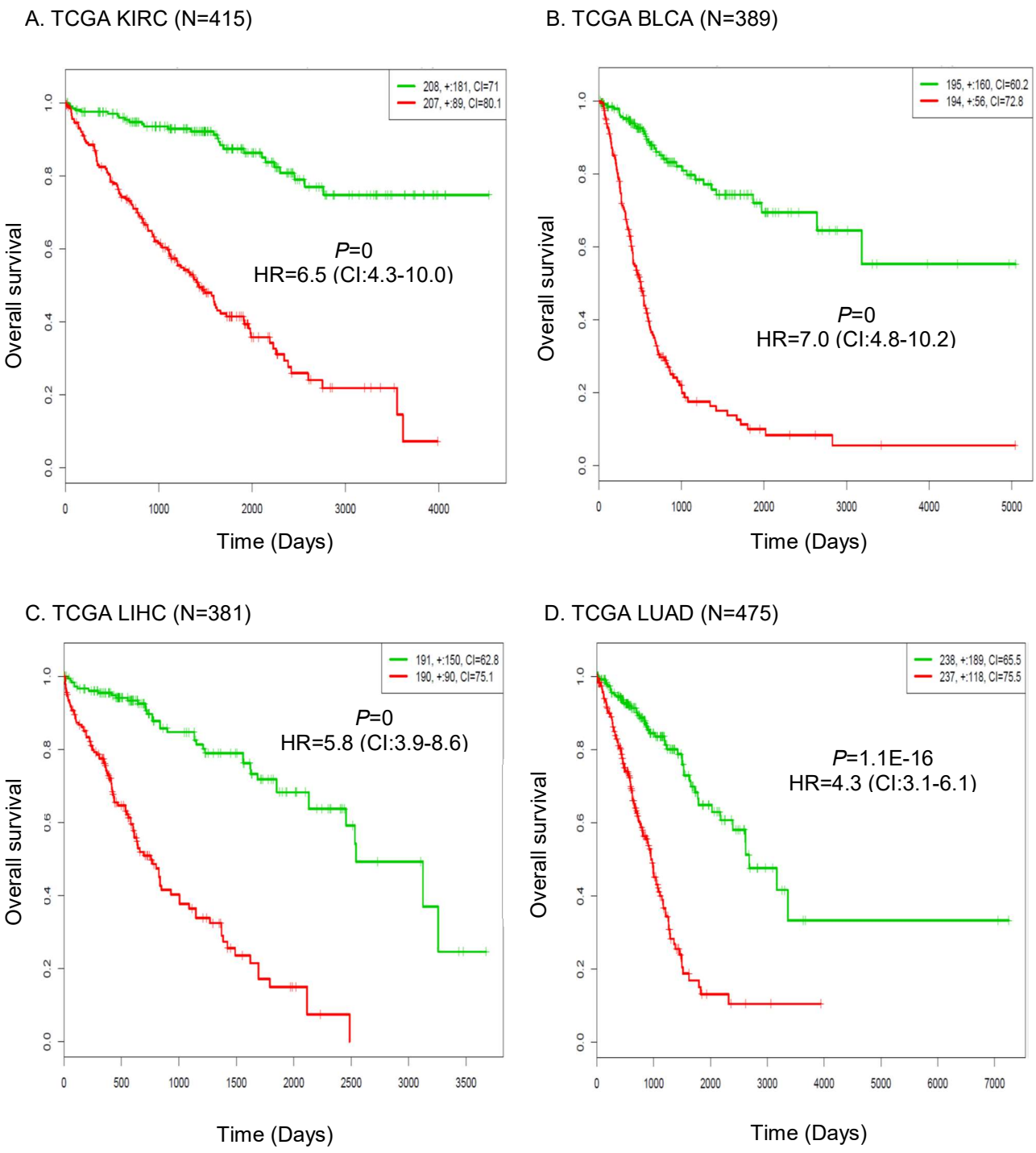

Figure S11. Kaplan–Meier analysis showed that the 121-gene set classifier can separate significantly low- and high-risk groups in the 13 major TCGA cancers. Related to Figure 9. The Kaplan–Meier curves of the TCGA cancer types of (A) KIRC, (B) BLCA, (C) LIHC, (D) LUAD were shown in this figure.

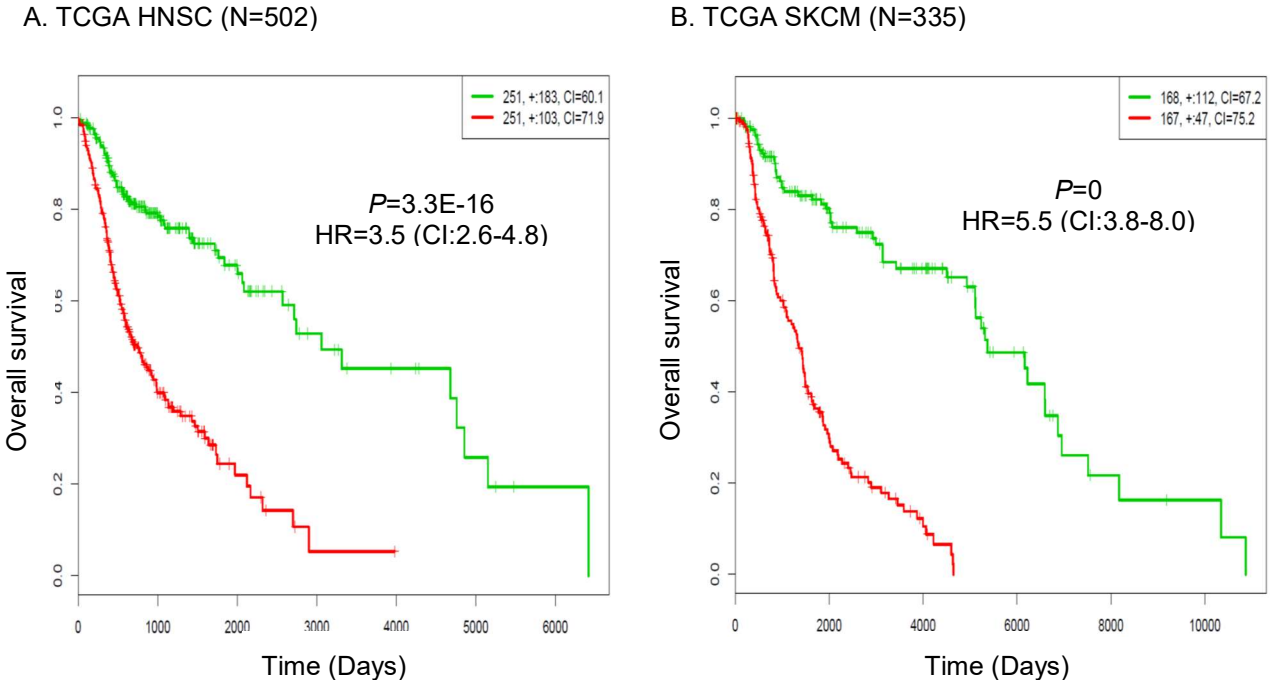

Figure S12. Kaplan–Meier analysis showed that the 121-gene set classifier can separate significantly low- and high-risk groups in the 13 major TCGA cancers. Related to Figure 9. The Kaplan–Meier curves of the TCGA cancer types of (A) HNSC, (B) SKCM were shown in this figure.

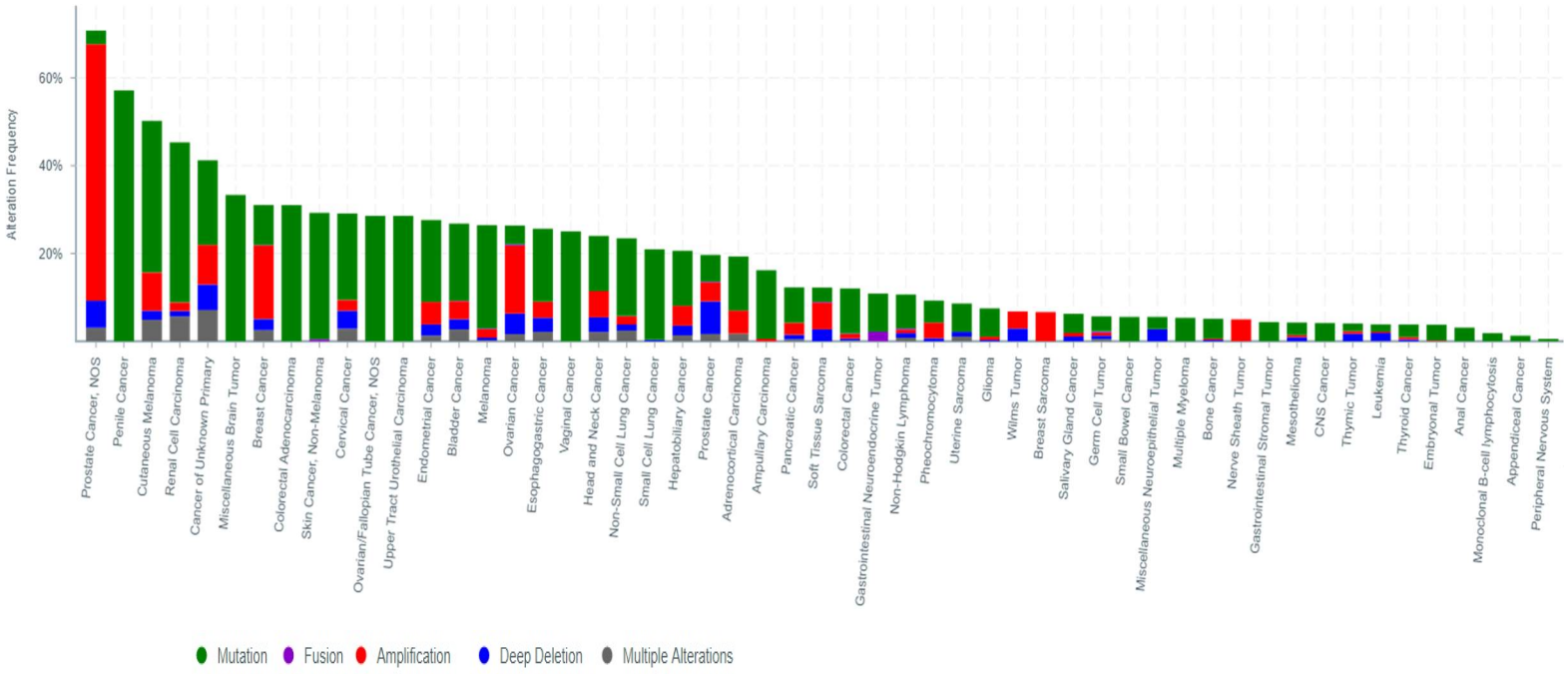

Figure S13. The mutation analysis highlighted eleven genes with deleterious mutations in the HPD tumors after anti-PD-1 therapy. Related to Table 2. Most of these genes have not been adequately studied in the cancer context before. Querying the HPD tumors associated 11-mutated-gene set in the cBioPortal website (http://www.cbioportal.org/) showed that this gene set had somatic mutations or copy number aberrations (CNAs) in 8887 (22%) of 41320 sequenced patients. The frequencies of tumor samples having somatic alterations in at least one of the eleven genes among each type of cancers archived in cBioPortal were shown in the figure.

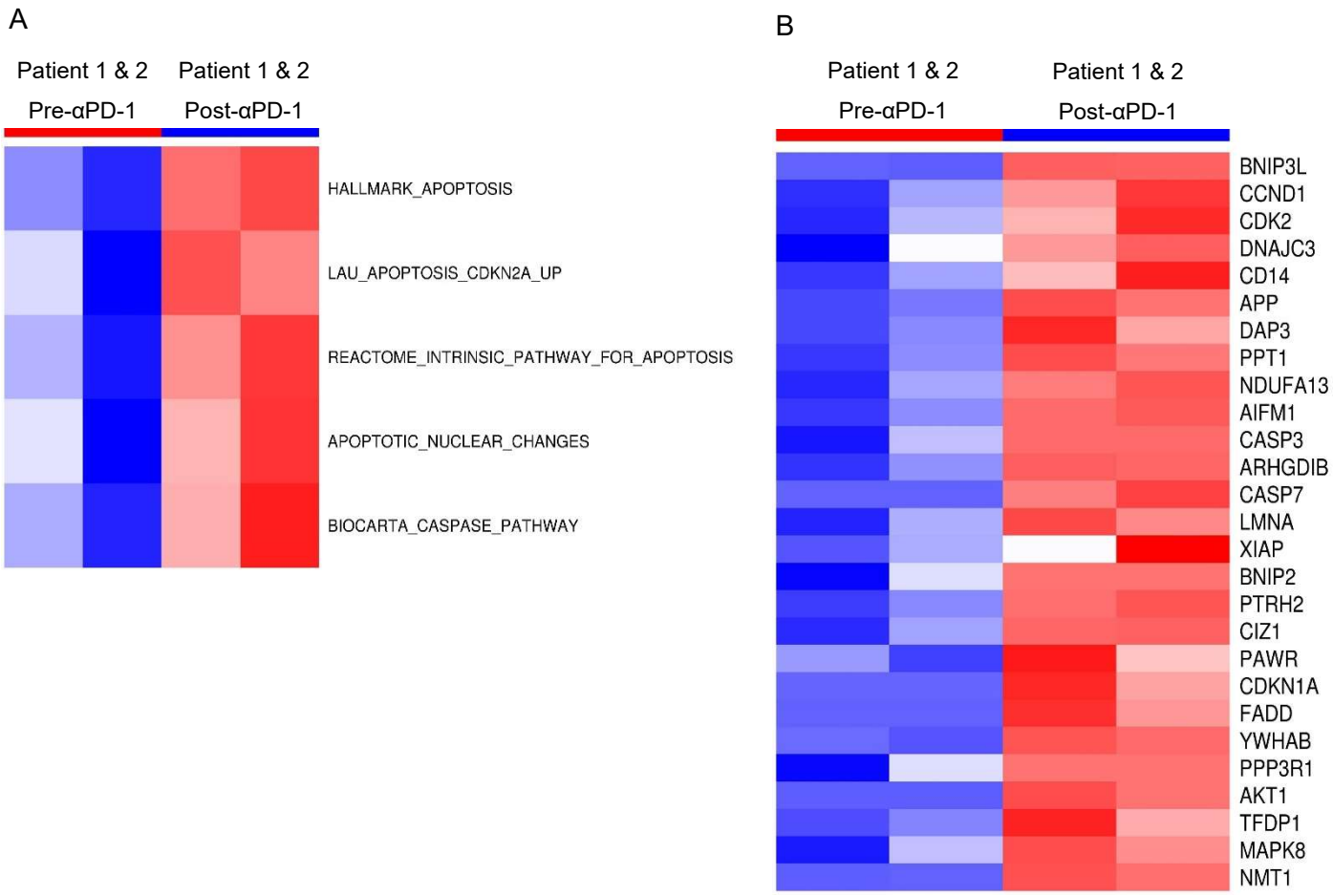

Figure S14. Changes of the apoptosis pathway activity in the after anti-PD-1 immunotherapy tumors of the HPD patients. Related to Figure 5 and Figure 6. (A) Five apoptosis gene sets were activated in the two patients after anti-PD-1 immunotherapy; (B) 27 apoptotic genes of these five apoptosis gene sets including marker genes in caspase/bcl2 pathways (CASP3, CASP7, BNIP2, BNIP3L) were significantly up-regulated.

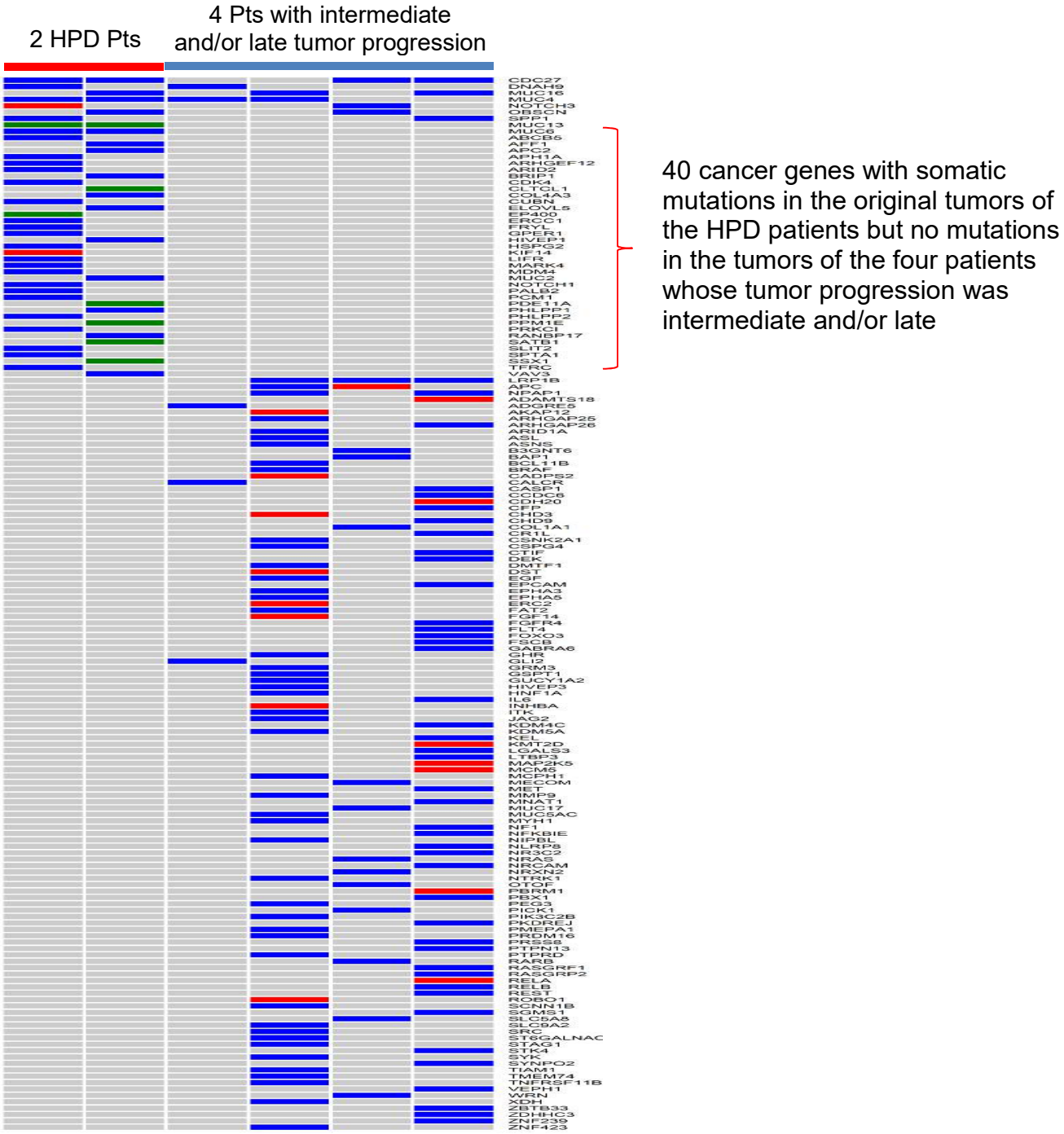

Figure S15. Comparison of the somatic mutation profiles of pretreatment tumor samples between HPD patients and a subset of non-HPD patients. Related to Figure 9. Mutation analysis showed that 40 cancer genes had somatic mutations in the original tumors of the HPD patients but no mutations in the tumors of the patients whose tumor progression was intermediate and/or late.

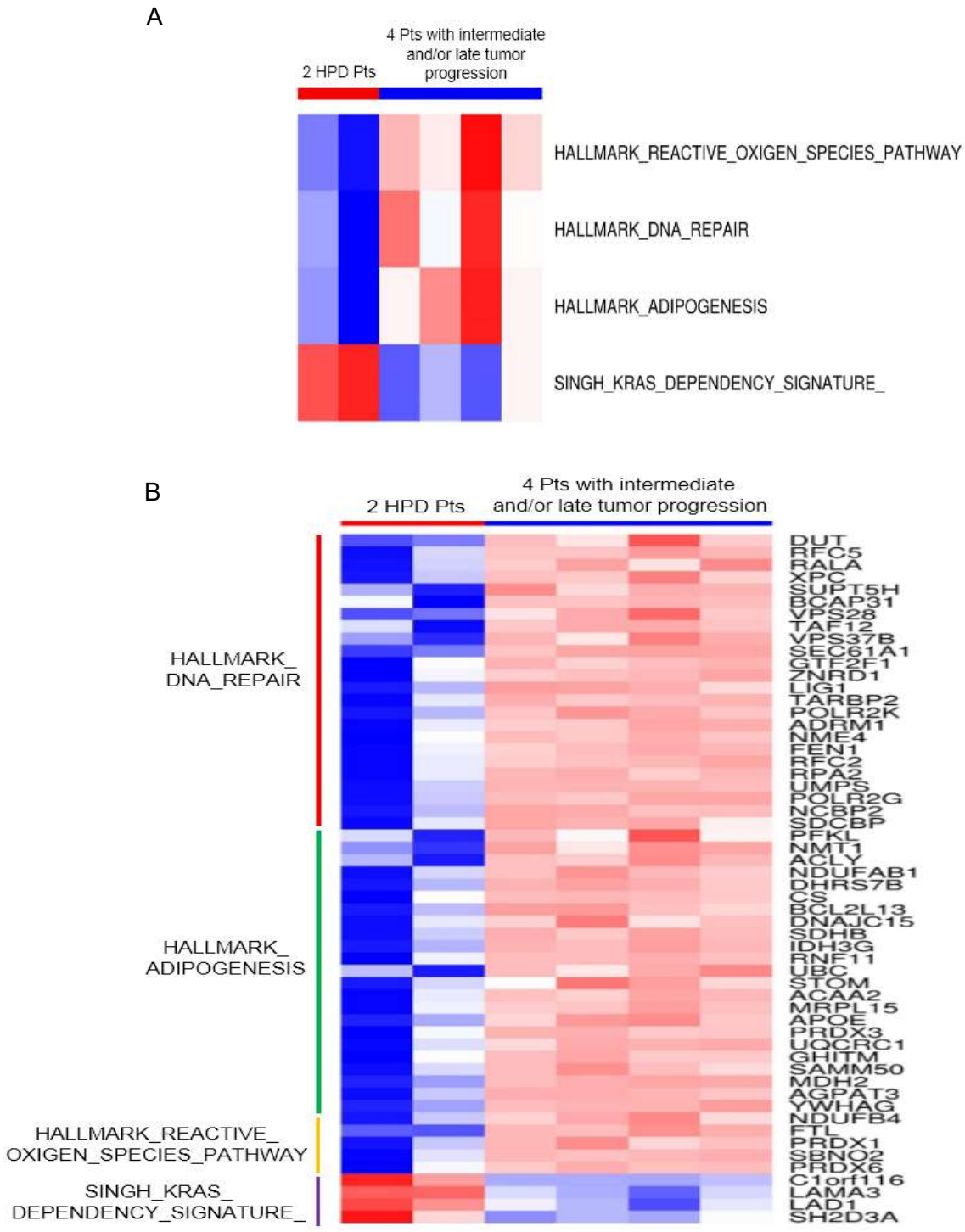

Figure S16. GSVA analysis of the transcriptional profiles of pretreatment tumor samples between HPD patients and a subset of non-HPD patients. Related to Figure 9. (A) Four gene sets were significantly altered in the tumors of HPD patients compared to the patients with intermediate and/or late tumor progression; (B) The corresponding gene expression changes of the above significantly altered pathways were also shown.

Table S1, Table S2, Table S3 were the supplemental Excel files.

Table S4. The clinical information of the eighteen follicular lymphoma patients from the GSE52562 study, among whom two patients had PFS less than two months together with advanced tumor progression phenotypes after anti-PD-1 treatment. Related to Figure 9.

ExpId	SampleID	gender	age	pfs.censorship	pfs.time.month	treatment	tissue	HPDstatus
GSM1269893	SAMPLE.25	F	67	1	1.8	pre-pidilizumab	tumor biopsy	HPD
GSM1269873	SAMPLE.5	F	79	1	2.0	pre-pidilizumab	tumor biopsy	HPD
GSM1269883	SAMPLE.15	M	46	1	3.7	pre-pidilizumab	tumor biopsy	nonHPD
GSM1269886	SAMPLE.18	M	69	0	4.1	pre-pidilizumab	tumor biopsy	nonHPD
GSM1269877	SAMPLE.9	F	58	1	6.5	pre-pidilizumab	tumor biopsy	nonHPD
GSM1269888	SAMPLE.20	F	56	0	7.1	pre-pidilizumab	tumor biopsy	nonHPD
GSM1269875	SAMPLE.7	M	60	1	10.1	pre-pidilizumab	tumor biopsy	nonHPD
GSM1269889	SAMPLE.21	F	62	1	12.7	pre-pidilizumab	tumor biopsy	nonHPD
GSM1269871	SAMPLE.3	M	51	1	13.5	pre-pidilizumab	tumor biopsy	nonHPD
GSM1269894	SAMPLE.26	M	58	1	15.3	pre-pidilizumab	tumor biopsy	nonHPD
GSM1269890	SAMPLE.22	M	70	1	18.6	pre-pidilizumab	tumor biopsy	nonHPD
GSM1269892	SAMPLE.24	M	63	0	18.8	pre-pidilizumab	tumor biopsy	nonHPD
GSM1269879	SAMPLE.11	M	67	1	19.6	pre-pidilizumab	tumor biopsy	nonHPD
GSM1269869	SAMPLE.1	F	61	1	21.6	pre-pidilizumab	tumor biopsy	nonHPD
GSM1269891	SAMPLE.23	F	37	0	26.5	pre-pidilizumab	tumor biopsy	nonHPD
GSM1269887	SAMPLE.19	F	41	0	30.4	pre-pidilizumab	tumor biopsy	nonHPD
GSM1269881	SAMPLE.13	M	58	0	30.8	pre-pidilizumab	tumor biopsy	nonHPD
GSM1269885	SAMPLE.17	F	45	0	35.0	pre-pidilizumab	tumor biopsy	nonHPD

Table S5. The information of the 121 genes in the expression signature of pre-anti-PD-1 treatment tumors that may be predictive of HPD (hyperprogressive disease) patients after anti-PD-1 immunotherapy. Related to Figure 9.

Gene Symbol	Entrez Gene Name	Location	Type(s)
AAK1	AP2 associated kinase 1	Cytoplasm	kinase
ACOT1	acyl-CoA thioesterase 1	Cytoplasm	enzyme
ACOT2	acyl-CoA thioesterase 2	Cytoplasm	enzyme
ADAR	adenosine deaminase, RNA specific	Nucleus	enzyme
AFF1	AF4/FMR2 family member 1	Nucleus	transcription regulator
ANKS6	ankyrin repeat and sterile alpha motif domain containing 6	Cytoplasm	other
ANXA5	annexin A5	Plasma Membrane	transporter
ARID2	AT-rich interaction domain 2	Nucleus	transcription regulator

ARL1	ADP ribosylation factor like GTPase 1	Cytoplasm	enzyme
ARMC9	armadillo repeat containing 9	Cytoplasm	other
ATF7IP	activating transcription factor 7 interacting protein	Nucleus	transcription regulator
ATP11C	ATPase phospholipid transporting 11C	Plasma Membrane	transporter
ATP5L	ATP synthase membrane subunit g	Cytoplasm	enzyme
BAZ1B	bromodomain adjacent to zinc finger domain 1B	Nucleus	transcription regulator
BAZ2A	bromodomain adjacent to zinc finger domain 2A	Nucleus	transcription regulator
C17orf97	chromosome 17 open reading frame 97	Other	other
CAMSAP1	calmodulin regulated spectrin associated protein 1	Cytoplasm	other
CARD8	caspase recruitment domain family member 8	Nucleus	other
CCNA1	cyclin A1	Nucleus	other
CCNT1	cyclin T1	Nucleus	transcription regulator
CD63	CD63 molecule	Plasma Membrane	other
CD96	CD96 molecule	Plasma Membrane	other
CHD4	chromodomain helicase DNA binding protein 4	Nucleus	enzyme
CLSTN3	calsyntenin 3	Plasma Membrane	other
COL4A1	collagen type IV alpha 1 chain	Extracellular Space	other
COL4A2	collagen type IV alpha 2 chain	Extracellular Space	other
COMMD9	COMM domain containing 9	Cytoplasm	other
CORO1C	coronin 1C	Cytoplasm	other
CPT1A	carnitine palmitoyltransferase 1A	Cytoplasm	enzyme
CREBZF	CREB/ATF bZIP transcription factor	Nucleus	transcription regulator
CSNK1G1	casein kinase 1 gamma 1	Cytoplasm	kinase
CTLA4	cytotoxic T-lymphocyte associated protein 4	Plasma Membrane	transmembrane receptor
CYP2D6	cytochrome P450 family 2 subfamily D member 6	Cytoplasm	enzyme
DGKD	diacylglycerol kinase delta	Cytoplasm	kinase
DIAPH1	diaphanous related formin 1	Plasma Membrane	other
EID2	EP300 interacting inhibitor of differentiation 2	Nucleus	other
ELK4	ELK4, ETS transcription factor	Nucleus	transcription regulator
EP300	E1A binding protein p300	Nucleus	transcription regulator
ERN1	endoplasmic reticulum to nucleus signaling 1	Cytoplasm	kinase
FAHD1	fumarylacetoacetate hydrolase domain containing 1	Cytoplasm	enzyme
FAM104B	family with sequence similarity 104 member B	Other	other
FBXL17	F-box and leucine rich repeat protein 17	Other	other

FPGT	fucose-1-phosphate guanylyltransferase	Cytoplasm	enzyme
FUBP3	far upstream element binding protein 3	Nucleus	transcription regulator
FUCA2	alpha-L-fucosidase 2	Extracellular Space	enzyme
GALNT10	polypeptide N-acetylgalactosaminyltransferase 10	Cytoplasm	enzyme
GALNT2	polypeptide N-acetylgalactosaminyltransferase 2	Cytoplasm	enzyme
GAPVD1	GTPase activating protein and VPS9 domains 1	Cytoplasm	other
GATAD2B	GATA zinc finger domain containing 2B	Nucleus	transcription regulator
GBF1	golgi brefeldin A resistant guanine nucleotide exchange factor 1	Cytoplasm	other
GOLIM4	golgi integral membrane protein 4	Cytoplasm	other
GPR18	G protein-coupled receptor 18	Plasma Membrane	G-protein coupled receptor
HADH	hydroxyacyl-CoA dehydrogenase	Cytoplasm	enzyme
HHLA3	HERV-H LTR-associating 3	Other	other
HIVEP1	human immunodeficiency virus type I enhancer binding protein 1	Nucleus	transcription regulator
HIVEP2	human immunodeficiency virus type I enhancer binding protein 2	Nucleus	transcription regulator
HMBS	hydroxymethylbilane synthase	Cytoplasm	enzyme
HPGDS	hematopoietic prostaglandin D synthase	Cytoplasm	enzyme
HSPG2	heparan sulfate proteoglycan 2	Extracellular Space	enzyme
KDM6B	lysine demethylase 6B	Extracellular Space	enzyme
KDR	kinase insert domain receptor	Plasma Membrane	kinase
KLHDC8B	kelch domain containing 8B	Cytoplasm	other
LAMTOR3	late endosomal/lysosomal adaptor, MAPK and MTOR activator 3	Cytoplasm	other
LGALS12	galectin 12	Extracellular Space	other
LNPEP	leucyl and cystinyl aminopeptidase	Cytoplasm	peptidase
LRP6	LDL receptor related protein 6	Plasma Membrane	transmembrane receptor
MAGEH1	MAGE family member H1	Cytoplasm	other
MEF2D	myocyte enhancer factor 2D	Nucleus	transcription regulator
MTIF3	mitochondrial translational initiation factor 3	Cytoplasm	translation regulator
NFE2L2	nuclear factor, erythroid 2 like 2	Nucleus	transcription regulator
NOTCH3	notch 3	Plasma Membrane	transcription regulator
NPLOC4	NPL4 homolog, ubiquitin recognition factor	Nucleus	other
NSD1	nuclear receptor binding SET domain protein 1	Nucleus	transcription regulator
NUP188	nucleoporin 188	Nucleus	other
OBSCN	obscurin, cytoskeletal calmodulin and titin-interacting RhoGEF	Cytoplasm	kinase
OTUD7B	OTU deubiquitinase 7B	Cytoplasm	peptidase

PAK2	p21 (RAC1) activated kinase 2	Cytoplasm	kinase
PCDHGB7	protocadherin gamma subfamily B, 7	Other	other
PHF8	PHD finger protein 8	Nucleus	enzyme
PPM1L	protein phosphatase, Mg2+/Mn2+ dependent 1L	Cytoplasm	phosphatase
PPP2R3C	protein phosphatase 2 regulatory subunit B''gamma	Cytoplasm	other
PTPN3	protein tyrosine phosphatase, non-receptor type 3	Cytoplasm	phosphatase
PTS	6-pyruvoyltetrahydropterin synthase	Cytoplasm	enzyme
RANGAP1	Ran GTPase activating protein 1	Nucleus	other
SATB1	SATB homeobox 1	Nucleus	transcription regulator
SERPINF1	serpin family F member 1	Extracellular Space	other
SETX	senataxin	Nucleus	enzyme
SLC25A34	solute carrier family 25 member 34	Cytoplasm	other
SLC27A1	solute carrier family 27 member 1	Plasma Membrane	transporter
SLC38A6	solute carrier family 38 member 6	Plasma Membrane	transporter
SLC6A6	solute carrier family 6 member 6	Plasma Membrane	transporter
SMURF1	SMAD specific E3 ubiquitin protein ligase 1	Cytoplasm	enzyme
SNAPC4	small nuclear RNA activating complex polypeptide 4	Nucleus	transcription regulator
SORT1	sortilin 1	Plasma Membrane	G-protein coupled receptor
SPEN	spen family transcriptional repressor	Nucleus	transcription regulator
SPIN2A	spindlin family member 2A	Other	other
SPP1	secreted phosphoprotein 1	Extracellular Space	cytokine
SSBP2	single stranded DNA binding protein 2	Nucleus	transcription regulator
OBFC1	STN1, CST complex subunit	Nucleus	other
SYTL4	synaptotagmin like 4	Cytoplasm	transporter
TCF4	transcription factor 4	Nucleus	transcription regulator
TEX261	testis expressed 261	Extracellular Space	other
TGOLN2	trans-golgi network protein 2	Cytoplasm	other
TIMM8B	translocase of inner mitochondrial membrane 8 homolog B	Cytoplasm	transporter
TLN1	talin 1	Plasma Membrane	other
TMEM99	transmembrane protein 99	Other	other
TNFRSF25	TNF receptor superfamily member 25	Plasma Membrane	transmembrane receptor
TNKS2	tankyrase 2	Nucleus	enzyme
TRIO	trio Rho guanine nucleotide exchange factor	Cytoplasm	kinase
TRIP12	thyroid hormone receptor interactor 12	Cytoplasm	enzyme
TSC2	TSC complex subunit 2	Cytoplasm	other
TSPAN3	tetraspanin 3	Plasma Membrane	other

UBTF	upstream binding transcription factor, RNA polymerase I	Nucleus	transcription regulator
KIAA2018	upstream transcription factor family member 3	Other	other
VHL	von Hippel-Lindau tumor suppressor	Nucleus	transcription regulator
WDR44	WD repeat domain 44	Cytoplasm	other
YWHAE	tyrosine 3-monooxygenase/tryptophan 5-monooxygenase activation protein epsilon	Cytoplasm	other
YWHAQ	tyrosine 3-monooxygenase/tryptophan 5-monooxygenase activation protein theta	Cytoplasm	other
ZFP36L1	ZFP36 ring finger protein like 1	Nucleus	transcription regulator
ZNF609	zinc finger protein 609	Nucleus	other
ZNF878	zinc finger protein 878	Other	other

Table S6. The clinical information of the 51 melanoma patients subjected to nivolumab immunotherapy from the CA209-038 study, among whom 21 patients had PFS less than two months together with post-therapy tumor progression phenotypes. Related to Figure 9.

PatientID	Sample	SampleType	PFS Censorship	Clinical Phenotype	PFS (days)	HPD status
Pt103	Pt103_Pre	Pre-anti-PD-1 tumor	0	PROGRESSION	50	HPD
Pt106	Pt106_Pre	Pre-anti-PD-1 tumor	0	PROGRESSION	56	HPD
Pt11	Pt11_Pre	Pre-anti-PD-1 tumor	0	PROGRESSION	59	HPD
Pt17	Pt17_Pre	Pre-anti-PD-1 tumor	0	PROGRESSION	48	HPD
Pt1	Pt1_Pre	Pre-anti-PD-1 tumor	0	PROGRESSION	54	HPD
Pt24	Pt24_Pre	Pre-anti-PD-1 tumor	0	PROGRESSION	50	HPD
Pt27	Pt27_Pre	Pre-anti-PD-1 tumor	0	PROGRESSION	50	HPD
Pt29	Pt29_Pre	Pre-anti-PD-1 tumor	0	PROGRESSION	50	HPD
Pt31	Pt31_Pre	Pre-anti-PD-1 tumor	0	PROGRESSION	50	HPD
Pt39	Pt39_Pre	Pre-anti-PD-1 tumor	0	PROGRESSION	57	HPD
Pt46	Pt46_Pre	Pre-anti-PD-1 tumor	0	PROGRESSION	51	HPD
Pt47	Pt47_Pre	Pre-anti-PD-1 tumor	0	PROGRESSION	57	HPD
Pt52	Pt52_Pre	Pre-anti-PD-1 tumor	0	PROGRESSION	57	HPD
Pt5	Pt5_Pre	Pre-anti-PD-1 tumor	0	PROGRESSION	56	HPD
Pt62	Pt62_Pre	Pre-anti-PD-1 tumor	0	PROGRESSION	56	HPD
Pt66	Pt66_Pre	Pre-anti-PD-1 tumor	0	PROGRESSION	59	HPD
Pt78	Pt78_Pre	Pre-anti-PD-1 tumor	0	PROGRESSION	50	HPD
Pt84	Pt84_Pre	Pre-anti-PD-1 tumor	0	PROGRESSION	50	HPD
Pt85	Pt85_Pre	Pre-anti-PD-1 tumor	0	PROGRESSION	49	HPD
Pt8	Pt8_Pre	Pre-anti-PD-1 tumor	0	PROGRESSION	52	HPD
Pt90	Pt90_Pre	Pre-anti-PD-1 tumor	0	PROGRESSION	44	HPD
Pt101	Pt101_Pre	Pre-anti-PD-1 tumor	0	PARTIAL RESPONSE	612	nonHPD
Pt10	Pt10_Pre	Pre-anti-PD-1 tumor	0	STABLE DISEASE	119	nonHPD
Pt18	Pt18_Pre	Pre-anti-PD-1 tumor	0	NA	519	nonHPD
Pt23	Pt23_Pre	Pre-anti-PD-1 tumor	0	DEATH PRIOR TO DISEASE ASSESSMENT	52	nonHPD
Pt26	Pt26_Pre	Pre-anti-PD-1 tumor	0	PROGRESSION	294	nonHPD
Pt28	Pt28_Pre	Pre-anti-PD-1 tumor	0	PROGRESSION	61	nonHPD
Pt2	Pt2_Pre	Pre-anti-PD-1 tumor	1	STABLE DISEASE	115	nonHPD
Pt30	Pt30_Pre	Pre-anti-PD-1 tumor	0	PARTIAL RESPONSE	603	nonHPD
Pt34	Pt34_Pre	Pre-anti-PD-1 tumor	1	NA	834	nonHPD
Pt36	Pt36_Pre	Pre-anti-PD-1 tumor	1	NA	737	nonHPD
Pt37	Pt37_Pre	Pre-anti-PD-1 tumor	0	STABLE DISEASE	176	nonHPD
Pt38	Pt38_Pre	Pre-anti-PD-1 tumor	0	PROGRESSION	167	nonHPD
Pt3	Pt3_Pre	Pre-anti-PD-1 tumor	0	PARTIAL RESPONSE	583	nonHPD
Pt44	Pt44_Pre	Pre-anti-PD-1 tumor	0	PARTIAL RESPONSE	560	nonHPD
Pt48	Pt48_Pre	Pre-anti-PD-1 tumor	1	NA	1046	nonHPD
Pt49	Pt49_Pre	Pre-anti-PD-1 tumor	1	PARTIAL RESPONSE	827	nonHPD
Pt4	Pt4_Pre	Pre-anti-PD-1 tumor	0	STABLE DISEASE	175	nonHPD
Pt59	Pt59_Pre	Pre-anti-PD-1 tumor	0	STABLE DISEASE	111	nonHPD
Pt65	Pt65_Pre	Pre-anti-PD-1 tumor	1	STABLE DISEASE	280	nonHPD
Pt67	Pt67_Pre	Pre-anti-PD-1 tumor	0	STABLE DISEASE	281	nonHPD
Pt72	Pt72_Pre	Pre-anti-PD-1 tumor	0	PARTIAL RESPONSE	333	nonHPD
Pt76	Pt76_Pre	Pre-anti-PD-1 tumor	0	NA	10	nonHPD

Pt77	Pt77_Pre	Pre-anti-PD-1 tumor	0	STABLE DISEASE	163	nonHPD
Pt79	Pt79_Pre	Pre-anti-PD-1 tumor	0	STABLE DISEASE	171	nonHPD
Pt82	Pt82_Pre	Pre-anti-PD-1 tumor	0	STABLE DISEASE	220	nonHPD
Pt89	Pt89_Pre	Pre-anti-PD-1 tumor	0	STABLE DISEASE	219	nonHPD
Pt92	Pt92_Pre	Pre-anti-PD-1 tumor	0	STABLE DISEASE	190	nonHPD
Pt94	Pt94_Pre	Pre-anti-PD-1 tumor	1	COMPLETE RESPONSE	729	nonHPD
Pt98	Pt98_Pre	Pre-anti-PD-1 tumor	0	STABLE DISEASE	408	nonHPD
Pt9	Pt9_Pre	Pre-anti-PD-1 tumor	0	PROGRESSION	66	nonHPD

Table S7. The information of the 40 HPD associated cancer genes having nonsilent somatic mutations in the original tumors of the HPD patients but no mutations in the tumors of the patients whose tumor progression was intermediate and/or late. Related to Figure 9.

Symbol	Entrez Gene Name	Location	Type(s)
ABCB5	ATP binding cassette subfamily B member 5	Plasma Membrane	transporter
AFF1	AF4/FMR2 family member 1	Nucleus	transcription regulator
APC2	APC2, WNT signaling pathway regulator	Cytoplasm	enzyme
APH1A	aph-1 homolog A, gamma-secretase subunit	Cytoplasm	peptidase
ARHGEF12	Rho guanine nucleotide exchange factor 12	Cytoplasm	other
ARID2	AT-rich interaction domain 2	Nucleus	transcription regulator
BRIP1	BRCA1 interacting protein C-terminal helicase 1	Nucleus	enzyme
CDK4	cyclin dependent kinase 4	Nucleus	kinase
CLTCL1	clathrin heavy chain like 1	Plasma Membrane	other
COL4A3	collagen type IV alpha 3 chain	Extracellular Space	other
CUBN	cubilin	Plasma Membrane	transmembrane receptor
ELOVL5	ELOVL fatty acid elongase 5	Cytoplasm	enzyme
EP400	E1A binding protein p400	Nucleus	other
ERCC1	ERCC excision repair 1, endonuclease non-catalytic subunit	Nucleus	enzyme
FRYL	FRY like transcription coactivator	Other	other
GPER1	G protein-coupled estrogen receptor 1	Plasma Membrane	G-protein coupled receptor
HIVEP1	human immunodeficiency virus type I enhancer binding protein 1	Nucleus	transcription regulator
HSPG2	heparan sulfate proteoglycan 2	Extracellular Space	enzyme
KIF14	kinesin family member 14	Cytoplasm	enzyme
LIFR	LIF receptor alpha	Plasma Membrane	transmembrane receptor
MARK4	microtubule affinity regulating kinase 4	Cytoplasm	kinase
MDM4	MDM4, p53 regulator	Nucleus	enzyme
MUC13	mucin 13, cell surface associated	Extracellular Space	other
MUC2	mucin 2, oligomeric mucus/gel-forming	Extracellular Space	other
MUC6	mucin 6, oligomeric mucus/gel-forming	Extracellular Space	other
NOTCH1	notch 1	Plasma Membrane	transcription regulator
PALB2	partner and localizer of BRCA2	Nucleus	other
PCM1	pericentriolar material 1	Cytoplasm	other
PDE11A	phosphodiesterase 11A	Cytoplasm	enzyme
PHLPP1	PH domain and leucine rich repeat protein phosphatase 1	Cytoplasm	enzyme
PHLPP2	PH domain and leucine rich repeat protein phosphatase 2	Cytoplasm	enzyme
PPM1E	protein phosphatase, Mg2+/Mn2+ dependent 1E	Nucleus	phosphatase
PRKCI	protein kinase C iota	Cytoplasm	kinase
RANBP17	RAN binding protein 17	Nucleus	transporter
SATB1	SATB homeobox 1	Nucleus	transcription regulator
SLIT2	slit guidance ligand 2	Extracellular Space	other
SPTA1	spectrin alpha, erythrocytic 1	Cytoplasm	other
SSX1	SSX family member 1	Nucleus	transcription regulator
TFRC	transferrin receptor	Plasma Membrane	transporter
VAV3	vav guanine nucleotide exchange factor 3	Extracellular Space	cytokine

Transparent Methods:

Whole-exome sequencing (WES) and RNA-seq experimentation and data analyses

For each set of paired tumor samples, a section of formalin-fixed tissue was examined with hematoxylin and eosin (H&E) staining to confirm the presence of tumor and determine the relative tumor burden. At least five 10-mm FFPE slides were used for each tumor specimen, from which DNA and RNA were purified by a commercial vendor (Omega Bio-tek, Inc., Norcross, GA 30071) and subjected to WES and RNA-seq after library purification. The Illumina Nextera Rapid Capture Exome kit was used for the preparation of exome libraries, which were sequenced to the average depth of 150 X coverage in the paired end 150 bp (PE150) mode with a HiSeq 4000 system. The Illumina TruSeq RNA Access kit was used for the preparation of total RNA libraries that were sequenced to the average depth of 75 million reads in the paired end 100 bp (PE100) mode using the HiSeq 2500 system.

The WES short reads were aligned to a reference genome (NCBI human genome assembly hg19) using the BWA (Burrows-Wheeler Aligner) program (Li and Durbin, 2009). Each alignment was assigned a mapping quality score by BWA (Li and Durbin, 2009), which generated a Phred-scaled probability that the alignment is correct. Reads with low mapping quality scores (< 5) were removed to reduce the false positive rate. The PCR duplicates were detected and removed using Picard software. Local realignment of the BWA-aligned reads was performed using the Genome Analysis Toolkit (GATK) (McKenna et al., 2010). VarScan 2 (Koboldt et al., 2012) was used to identify somatic variants based on the local realignment results comparing each tumor with the two reference blood samples. Default parameters in VarScan 2 were used. The lists of shared SNVs/indels were then annotated using ANNOVAR (Wang et al., 2010). Single nucleotide polymorphisms (SNPs) were filtered against dbSNP version 142 (dbSNP 142). Plots of mutations were generated using the “oncoPrint” function provided by the R package – ComplexHeatmap (Gu et al., 2016). To identify somatic mutations with the most significant functional consequences, we predicted the impact of the mutations on

HPD tumors using the bioinformatics programs SIFT, PolyPhen-2, and FATHMM according to our previous approaches (Xiong et al., 2015). Network analysis of the eleven genes having deleterious mutations in HPD tumors was performed and graphically depicted using Ingenuity Pathway Analysis software (IPA, QIAGEN Inc., https://www.qiagenbioinformatics.com/products/ingenuitypathway-analysis). Mapping of the p.Y1611S mutation to the 3D structure of the TSC2 protein was performed using MuPIT software (Niknafs et al., 2013). The bioinformatics tools SciClone (Miller et al., 2014) and Clonevol (Dang et al., 2017) were used to identify the clonal structures of the paired tumors of the two HPD patients. Plots of the clonal mutation clusters were generated using the fishplot software feature (Miller et al., 2016).

RNA-seq sample quality was analyzed using the FastQC program (http://www.bioinformatics.babraham.ac.uk/projects/fastqc/). Raw sequence data reads in fasta format were first processed through Perl scripts (Haas et al., 2013). Data were then refined by removing reads containing adapter, poly-N, or low-quality reads (Pei et al., 2016; Wang et al., 2015). All downstream analyses were based on refined data. The “rsem prepare reference” script of the RSEM package was used to generate reference transcript sequences by using the gene annotation file (GTF) format and the full genome sequence (FASTA) format of human GRCh37 assembly. All of the quality reads of different samples were mapped to generated reference transcript sequences using the Bowtie-2 program (Langmead et al., 2009) to determine the identity between cDNA sequences and corresponding genomic exons in regions of exact matches. The “rsem calculate expression” script of RSEM was used to analyze both the alignment of reads against reference transcript sequences and the calculation of relative abundances. Normalized gene expression values in TPM (Transcripts Per Kilobase Million) were used as input of the AltAnalyze software (Olsson et al., 2016) for differential gene expression analysis. FDR (False discovery rate) corrected *P*-values of less than 0.05 were used as criteria for significantly regulated genes.

To perform oncogenic pathway or network analysis, the list of differentially expressed genes between paired pre- and post-anti-PD-1 therapy tumors of the two patients was analyzed through the use of IPA. The GSVA (Gene Set Variation Analysis) (Hanzelmann et al., 2013) and GSEA (Gene Set Enrichment Analysis) (Subramanian et al., 2005) approaches were used to analyze the activity and enrichment of immune cell populations, respectively. GSEA analysis was performed for pre-ranked differentially expressed genes using the option 'GseaPreranked'. One thousand permutations were used to calculate significance. A gene set was considered to be significantly enriched in one of the two groups when the *P* value was lower than 0.05 and the FDR was lower than 0.25 for the corresponding gene set. For inflammatory pathway analysis, we performed a focused gene expression study by analyzing the changes of the inflammatory related genes included in the Hallmark gene set for inflammatory response named "HALLMARK_INFLAMMATORY_RESPONSE" downloaded from the MSigDB database (Liberzon et al., 2015; Liberzon et al., 2011). The GSVA approach (Hanzelmann et al., 2013) was used to characterize the activity of inflammation pathways in the post-anti-PD-1 treatment HPD tumors vs pre-treatment tumors. All heatmaps of gene expression were generated using the R package – heatmap3 (https://cran.r-project.org/web/packages/heatmap3/).

Tumor immunogenicity analysis

Immunogenicity of the pre-anti-PD-1 treatment tumors and post-treatment HPD tumors was analyzed using published criteria (Charoentong et al., 2017; Hakimi et al., 2016). The immunophenoscore (IPS) was calculated on an arbitrary 0–10 scale based on the sum of the weighted averaged Z score of the four categories shown in Figure 5 in accordance to the previous methods (Charoentong et al., 2017; Tappeiner et al., 2017). Briefly, the four categories include 20 single factors such as the presence of specific immune cell types along with the abundance of MHC molecules, or molecules known to act as immunoinhibitors or immunostimulators. For each determinant, a sample-wise Z score from gene expression data

was calculated. For the six cell types, an average Z score from the corresponding metagenes was calculated. The metagenes were defined previously as non-overlapping sets of genes that are representative for specific immune cell subpopulations and are not expressed in normal tissue (Charoentong et al., 2017). The detailed list of genes included in the metagenes were available from the same literature (Charoentong et al., 2017). The determinants were then divided into four categories—effector cells (activated CD4+ or CD8+ T cells and effector memory CD4+ T cells or CD8+ T cells), and suppressive cells (Tregs and MDSCs [myeloid-derived suppressor cells]), MHC-related molecules, and checkpoints or immunomodulators are color-coded in the outer part of the wheel (red: positive Z score, blue: negative Z score).

Development and validation of an HPD classifier based on gene expression data

Previously, no gene expression signature had been identified to predict which patients might develop HPD after receiving anti-PD-1 immunotherapy. To identify such predictors, we analyzed the publicly available gene expression data sets of the anti-PD-1 immunotherapy studies that may contain subsets of patients that acquired HPD. Similar to previous studies (Champiat et al., 2017; Kato et al., 2017; Saada-Bouzid et al., 2017), we defined HPD as (1) progression at first restaging on therapy, (2) increase in tumor size > 50%, and (3) >2-fold increase in tumor growth rate (TGR). Based on these criteria, we identified two cohorts in these datasets that received anti-PD-1 treatment and contained patients that developed putative HPD. The first study (Accession # “GSE52562” in the GEO database) performed gene expression profiling of tumor biopsies before and after pidilizumab (a humanized anti-PD-1 monoclonal antibody, also called “CT-011”) therapy in patients with relapsed follicular lymphoma (Westin et al., 2014). Previously, it was suggested that binding to PD-1 was the main driver for pidilizumab’s activity. Recent analyses show that pidilizumab binds to a hypoglycosylated /nonglycosylated form of PD-1 that is present on a distinct subpopulation of exhausted T cells (Fried et al., 2018). Nevertheless, multiple studies have shown that pidilizumab can affect PD-1 function either through binding or

other mechanisms, so pidilizumab treatment is still considered as anti-PD-1 therapy (Abdin et al., 2018; Benson et al., 2010; Jelinek and Hajek, 2016; Mkrtichyan et al., 2011; Rosenblatt et al., 2011; Westin et al., 2014). Two of eighteen follicular lymphoma patients from this study had PFS less than two months after anti-PD-1 treatment. These two patients were classified as HPD patients, while the other sixteen were non-HPD patients (Table S4). To develop an HPD-associated gene expression signature, the pre-therapy tumor expression data of our two HPD patients were combined with the pre-treatment tumor expression data of the two HPD patients and sixteen non-HPD patients from the GSE52562 study. This was used as the HPD signature discovery dataset (called “Dataset_1”). Another study (quoted as “CA209-038”) assessed transcriptome changes in tumors from the patients with advanced melanoma before and after nivolumab immunotherapy (Riaz et al., 2017). This CA209-038 study had 21 advanced melanoma patients having PFS < 2 months after anti-PD-1 immunotherapy. Therefore, these 21 patients were classified as the HPD patients while the other 31 patients were classified as non-HPD patients (Table S6). These 51 patients had pre-therapy gene expression data available, and this dataset was used as the validation dataset (called “Dataset_2”).

Based on the genome-wide expression data of Dataset_1 and Dataset_2, we developed and validated a 121-gene classifier using the *cancerclass* R package (Budczies et al., 2014). The performance of the 121-gene set as a classifier was evaluated with the use of receiver-operating-characteristic curves, calculation of AUC (Hanley and McNeil, 1982), and estimates of sensitivity and specificity implemented in the *cancerclass* R package (Jan et al., 2014). This classification protocol starts with a feature selection step and continues with nearest-centroid classification. Fisher’s exact test was used for categorical variables. All confidence intervals are reported as two-sided binomial 95% confidence intervals. Statistical analysis was performed with R software, version 3.2.3 (R Project for Statistical Computing). We also tested the prognostic performance of the 121-gene signature using gene expression data from the TCGA tumor samples in conjunction with the online biomarker validation tool and database –

SurvExpress (Aguirre-Gamboa et al., 2013). Specifically, Kaplan-Meier survival analyses were implemented to estimate the survival functions after the samples were classified into two risk groups according to their risk scores based on the 121-gene set. Differences in survival risk between the two risk groups were assessed using the Mantel-Haenszel log-rank test.

Supplemental References

Abdin, S.M., Zaher, D.M., Arafa, E.A., and Omar, H.A. (2018). Tackling Cancer Resistance by Immunotherapy: Updated Clinical Impact and Safety of PD-1/PD-L1 Inhibitors. Cancers (Basel) *10*.

Aguirre-Gamboa, R., Gomez-Rueda, H., Martinez-Ledesma, E., Martinez-Torteya, A., Chacolla-Huaringa, R., Rodriguez-Barrientos, A., Tamez-Pena, J.G., and Trevino, V. (2013). SurvExpress: an online biomarker validation tool and database for cancer gene expression data using survival analysis. PLoS One *8*, e74250.

Benson, D.M., Jr., Bakan, C.E., Mishra, A., Hofmeister, C.C., Efebera, Y., Becknell, B., Baiocchi, R.A., Zhang, J., Yu, J., Smith, M.K.*, et al.* (2010). The PD-1/PD-L1 axis modulates the natural killer cell versus multiple myeloma effect: a therapeutic target for CT-011, a novel monoclonal anti-PD-1 antibody. Blood *116*, 2286-2294.

Budczies, J., Kosztyla, D., Torne, C.V., Stenzinger, A., Darb-Esfahani, S., Dietel, M., and Denkert, C. (2014). cancerclass: An R Package for development and validation of diagnostic tests from high-dimensional molecular data. J Stat Software *59*, 1-19.

Champiat, S., Dercle, L., Ammari, S., Massard, C., Hollebecque, A., Postel-Vinay, S., Chaput, N., Eggermont, A., Marabelle, A., Soria, J.C.*, et al.* (2017). Hyperprogressive Disease Is a New Pattern of Progression in Cancer Patients Treated by Anti-PD-1/PD-L1. Clin Cancer Res *23*, 1920-1928.

Charoentong, P., Finotello, F., Angelova, M., Mayer, C., Efremova, M., Rieder, D., Hackl, H., and Trajanoski, Z. (2017). Pan-cancer Immunogenomic Analyses Reveal Genotype-Immunophenotype Relationships and Predictors of Response to Checkpoint Blockade. Cell Rep *18*, 248-262.

Dang, H.X., White, B.S., Foltz, S.M., Miller, C.A., Luo, J., Fields, R.C., and Maher, C.A. (2017). ClonEvol: clonal ordering and visualization in cancer sequencing. Ann Oncol *28*, 3076-3082.

Fried, I., Lossos, A., Ben Ami, T., Dvir, R., Toledano, H., Ben Arush, M.W., Postovski, S., Abu Kuidar, A., Yalon, M., Weintraub, M.*, et al.* (2018). Preliminary results of immune modulating antibody MDV9300 (pidilizumab) treatment in children with diffuse intrinsic pontine glioma. J Neurooncol *136*, 189-195.

Gu, Z., Eils, R., and Schlesner, M. (2016). Complex heatmaps reveal patterns and correlations in multidimensional genomic data. Bioinformatics *32*, 2847-2849.

Haas, B.J., Papanicolaou, A., Yassour, M., Grabherr, M., Blood, P.D., Bowden, J., Couger, M.B., Eccles, D., Li, B., Lieber, M.*, et al.* (2013). De novo transcript sequence reconstruction from RNA-seq using the Trinity platform for reference generation and analysis. Nat Protoc *8*, 1494-1512.

Hakimi, A.A., Reznik, E., Lee, C.H., Creighton, C.J., Brannon, A.R., Luna, A., Aksoy, B.A., Liu, E.M., Shen, R., Lee, W.*, et al.* (2016). An Integrated Metabolic Atlas of Clear Cell Renal Cell Carcinoma. Cancer Cell *29*, 104-116.

Hanley, J.A., and McNeil, B.J. (1982). The meaning and use of the area under a receiver operating characteristic (ROC) curve. Radiology *143*, 29-36.

Hanzelmann, S., Castelo, R., and Guinney, J. (2013). GSVA: gene set variation analysis for microarray and RNA-seq data. BMC Bioinformatics *14*, 7.

Jan, B., Kosztyla, D., von Törne, C., Stenzinger, A., Darb-Esfahani, S., Dietel, M., and Denkert, C. (2014). cancerclass: An R Package for Development and Validation of Diagnostic Tests from High-Dimensional Molecular Data. 2014 *59*, 19.

Jelinek, T., and Hajek, R. (2016). PD-1/PD-L1 inhibitors in multiple myeloma: The present and the future. Oncoimmunology *5*, e1254856.

Kato, S., Goodman, A., Walavalkar, V., Barkauskas, D.A., Sharabi, A., and Kurzrock, R. (2017). Hyperprogressors after Immunotherapy: Analysis of Genomic Alterations Associated with Accelerated Growth Rate. Clin Cancer Res *23*, 4242-4250.

Koboldt, D.C., Zhang, Q., Larson, D.E., Shen, D., McLellan, M.D., Lin, L., Miller, C.A., Mardis, E.R., Ding, L., and Wilson, R.K. (2012). VarScan 2: somatic mutation and copy number alteration discovery in cancer by exome sequencing. Genome Res *22*, 568-576.

Langmead, B., Trapnell, C., Pop, M., and Salzberg, S.L. (2009). Ultrafast and memory-efficient alignment of short DNA sequences to the human genome. Genome Biol *10*, R25.

Li, H., and Durbin, R. (2009). Fast and accurate short read alignment with Burrows-Wheeler transform. Bioinformatics *25*, 1754-1760.

Liberzon, A., Birger, C., Thorvaldsdottir, H., Ghandi, M., Mesirov, J.P., and Tamayo, P. (2015). The Molecular Signatures Database (MSigDB) hallmark gene set collection. Cell Syst *1*, 417-425.

Liberzon, A., Subramanian, A., Pinchback, R., Thorvaldsdottir, H., Tamayo, P., and Mesirov, J.P. (2011). Molecular signatures database (MSigDB) 3.0. Bioinformatics *27*, 1739-1740.

McKenna, A., Hanna, M., Banks, E., Sivachenko, A., Cibulskis, K., Kernytsky, A., Garimella, K., Altshuler, D., Gabriel, S., Daly, M.*, et al.* (2010). The Genome Analysis Toolkit: a MapReduce framework for analyzing next-generation DNA sequencing data. Genome Res *20*, 1297-1303.

Miller, C.A., McMichael, J., Dang, H.X., Maher, C.A., Ding, L., Ley, T.J., Mardis, E.R., and Wilson, R.K. (2016). Visualizing tumor evolution with the fishplot package for R. BMC Genomics *17*, 880.

Miller, C.A., White, B.S., Dees, N.D., Griffith, M., Welch, J.S., Griffith, O.L., Vij, R., Tomasson, M.H., Graubert, T.A., Walter, M.J.*, et al.* (2014). SciClone: inferring clonal architecture and tracking the spatial and temporal patterns of tumor evolution. PLoS Comput Biol *10*, e1003665.

Mkrtichyan, M., Najjar, Y.G., Raulfs, E.C., Abdalla, M.Y., Samara, R., Rotem-Yehudar, R., Cook, L., and Khleif, S.N. (2011). Anti-PD-1 synergizes with cyclophosphamide to induce potent anti-tumor vaccine effects through novel mechanisms. Eur J Immunol *41*, 2977-2986.

Niknafs, N., Kim, D., Kim, R., Diekhans, M., Ryan, M., Stenson, P.D., Cooper, D.N., and Karchin, R. (2013). MuPIT interactive: webserver for mapping variant positions to annotated, interactive 3D structures. Hum Genet *132*, 1235-1243.

Olsson, A., Venkatasubramanian, M., Chaudhri, V.K., Aronow, B.J., Salomonis, N., Singh, H., and Grimes, H.L. (2016). Single-cell analysis of mixed-lineage states leading to a binary cell fate choice. Nature *537*, 698-702.

Pei, M., Niu, J., Li, C., Cao, F., and Quan, S. (2016). Identification and expression analysis of genes related to calyx persistence in Korla fragrant pear. BMC Genomics *17*, 132.

Riaz, N., Havel, J.J., Makarov, V., Desrichard, A., Urba, W.J., Sims, J.S., Hodi, F.S., Martin-Algarra, S., Mandal, R., Sharfman, W.H.*, et al.* (2017). Tumor and Microenvironment Evolution during Immunotherapy with Nivolumab. Cell *171*, 934-949 e915.

Rosenblatt, J., Glotzbecker, B., Mills, H., Vasir, B., Tzachanis, D., Levine, J.D., Joyce, R.M., Wellenstein, K., Keefe, W., Schickler, M.*, et al.* (2011). PD-1 blockade by CT-011, anti-PD-1 antibody, enhances ex vivo T-cell responses to autologous dendritic cell/myeloma fusion vaccine. J Immunother *34*, 409-418.

Saada-Bouzid, E., Defaucheux, C., Karabajakian, A., Coloma, V.P., Servois, V., Paoletti, X., Even, C., Fayette, J., Guigay, J., Loirat, D.*, et al.* (2017). Hyperprogression during anti-PD-1/PD-L1 therapy in patients with recurrent and/or metastatic head and neck squamous cell carcinoma. Ann Oncol *28*, 1605-1611.

Subramanian, A., Tamayo, P., Mootha, V.K., Mukherjee, S., Ebert, B.L., Gillette, M.A., Paulovich, A., Pomeroy, S.L., Golub, T.R., Lander, E.S.*, et al.* (2005). Gene set enrichment analysis: a knowledge-based approach for interpreting genome-wide expression profiles. Proc Natl Acad Sci U S A *102*, 15545-15550.

Tappeiner, E., Finotello, F., Charoentong, P., Mayer, C., Rieder, D., and Trajanoski, Z. (2017). TIminer: NGS data mining pipeline for cancer immunology and immunotherapy. Bioinformatics *33*, 3140-3141.

Wang, K., Li, M., and Hakonarson, H. (2010). ANNOVAR: functional annotation of genetic variants from high-throughput sequencing data. Nucleic Acids Res *38*, e164.

Wang, X., Xiong, M., Lei, C., and Zhu, F. (2015). The developmental transcriptome of the synanthropic fly Chrysomya megacephala and insights into olfactory proteins. BMC Genomics *16*, 20.

Westin, J.R., Chu, F., Zhang, M., Fayad, L.E., Kwak, L.W., Fowler, N., Romaguera, J., Hagemeister, F., Fanale, M., Samaniego, F.*, et al.* (2014). Safety and activity of PD1 blockade

by pidilizumab in combination with rituximab in patients with relapsed follicular lymphoma: a single group, open-label, phase 2 trial. Lancet Oncol *15*, 69-77.

Xiong, D., Wang, Y., Kupert, E., Simpson, C., Pinney, S.M., Gaba, C.R., Mandal, D., Schwartz, A.G., Yang, P., de Andrade, M.*, et al.* (2015). A recurrent mutation in PARK2 is associated with familial lung cancer. Am J Hum Genet *96*, 301-308.